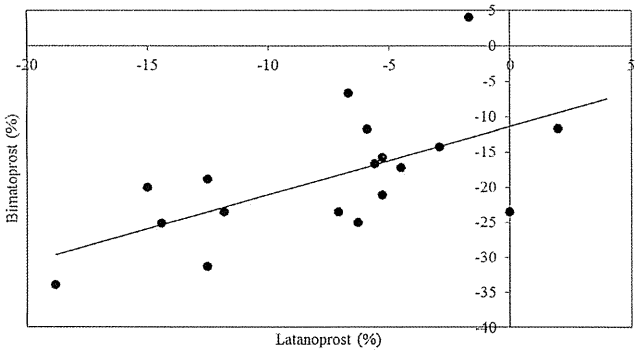

FIG. 3. Correlation between% IOP reduction rate of bimatoprost and latanoprost. % IOP reduction rate of bimatoprost was significantly correlated with that of latanoprost. (Pearson correlation coefficient $R^2=0.374$; $P=0.007$).

significant correlation between% IOP reduction of bimatoprost and that of latanoprost (Pearson correlation coefficient $r^2=0.374$; $P<0.01$) (Fig. 3).

The mean hyperemia scores at preswitch and week 12 were 0.31 ± 0.35 and 0.56 ± 0.54 ($P=0.27$), respectively (Table 1). The mean corneal epithelial disorder scores at preswitch and week 12 were 0.67 ± 0.97 and 0.67 ± 0.97 ($P>0.99$), respectively (Table 1).

Discussion

The incidence rate of latanoprost nonresponders is reported at 28.1% and was highest in patients with NTG in Japan.[18] The reduction of IOP in patients with lower baseline IOP may be more difficult.[20] Several studies revealed that the IOP-lowering effect of bimatoprost was even equal to or higher than that of latanoprost.[2,11–14]

Bimatoprost was difficult to be converted to its free acid form in human eyes, and free acid was slightly detected at the site of action in the eye.[8,21,22] In contrast, latanoprost is a prodrug that needs de-esterification to yield a pharmacologically active free fatty acid. Due to this, the pharmacological effect of bimatoprost is difficult to be attenuated because of its metabolism compared with latanoprost. Gandolfi and Cimino[14] previously reported that most of the subjects with glaucoma or OH who showed no significant IOP response to latanoprost were successfully treated with bimatoprost. They speculated that the lack of response to latanoprost was associated with poor de-esterification of the prodrug to the pharmacologically active free fatty acid. In early studies, the additional IOP-lowering effect of bimotoprost was seen in patients who responded poorly to latanoprost, thus suggesting a superior IOP-lowering effect of bimatoprost, compared with latanoprost.[14,23] Mean IOP before the switch to bimatoprost, however, was approximately 23 mm Hg in their study.[14,23] Our study suggests that the decrease of IOP also occurred with switching to bimatoprost in Japanese patients who are insufficient responders to latanoprost even though pretreatment IOP is low.

TABLE 1. MEAN CONJUNCTIVAL HYPEREMIA AND AREA DENSITY GRADING SCALE SCORES

	Mean conjunctival hyperemia	*Mean area density grading scale score*
Preswitch	0.31 ± 0.35	0.67 ± 0.97
At 4 weeks	0.47 ± 0.41 ($P=0.60$)	0.94 ± 1.20 ($P=0.78$)
At 8 weeks	0.50 ± 0.54 ($P=0.46$)	0.78 ± 1.00 ($P=0.98$)
At 12 weeks	0.56 ± 0.54 ($P=0.27$)	0.67 ± 0.97 ($P>0.99$)

In this study, we showed that the mean IOP reduction rate of bimatoprost was significantly correlated with the mean IOP reduction rate of latanoprost. Bimatoprost showed a trend to enhance the potency of latanoprost. Prostaglandin $F_{2\alpha}$ (FP) prostanoid receptors are G-protein coupled receptors that mediate the actions of PG $F_{2\alpha}$, which is confirmed to be an alternative splice variant of the human FP (altFP) prostanoid receptor gene.[24] Since bimatoprost interacts not with PG FP receptor but with prostamide receptor, bimatoprost is likely to have a pharmacologically inherent receptor.[7,8] It has been reported that bimatoprost may interact with the FP-altFP receptor heterodimer to induce alterations in second-messenger signaling.[25] FP-altFP complexes may represent the underlying basis of bimatoprost pharmacology.[25] Since prostamide and FP receptors may be encoded by the same gene, the lowering effects on IOP of bimatoprost might correlate with those of latanoprost.

Conjunctival hyperemia was the most commonly reported side effect of bimatoprost and the most frequently observed biomicroscopic finding in several studies.[2,3,14] Conjunctival hyperemia occurs more frequently with bimatoprost than with latanoprost.[26] There were, however, no significant differences in the mean score of conjunctival hyperemia between bimatoprost-treated eyes and latanoprost-treated eyes in this study. The switch from latanoprost to bimatoprost in the glaucoma therapy was associated with less conjunctival hyperemia than that measured in patients in whom bimatoprost was used as first-line therapy.[27] One of the limitations of this study is that there was no control group. There is the possibility that some patients who had conjunctival hyperemia caused by latanoprost may continue after withdrawal. Ocular surface hyperemia occurs by endothelial-derived nitric oxide-mediated vasodilatation and is not associated with intraocular inflammation.[28] Even though there is a trend toward exacerbation during the switching phase, no patients withdrew from the treatment. In addition, the deepening of eyelid sulcus due to bimatoprost has been reported.[29] Although 1 patient complained of the deepening of eyelid sulcus, the patient continued the treatment.

Low ocular perfusion pressure is an established risk factor in glaucoma.[30] Quaranta et al.[31] recently reported that in previously untreated patients with NTG, both latanoprost and bimatoprost reduced the IOP from untreated baseline, to a similar extent, over a 24-h curve. Latanoprost was associated with slightly improved ocular diastolic perfusion pressure over 24-h but similar absolute perfusion levels to those of bimatoprost.[31]

In conclusion, bimatoprost provided a significant reduction in IOP for at least 12 weeks for Japanese patients with NTG who showed insufficient response to latanoprost.

Author Disclosure Statement

No competing financial interests exist.

References

1. Whitcup, S.M., Cantor, L.B., VanDenburgh, A.M., and Chen, K. A randomized, double masked, multicentre clinical trial comparing bimatoprost and timolol for the treatment of

glaucoma and ocular hypertension. *Br. J. Ophthalmol.* 87:57–62, 2003.
2. Noecker, R.S., Dirks, M.S., Choplin, N.T., et al. Bimatoprost/Latanoprost Study Groupe. A six-month randomized clinical trial comparing the intraocular pressure-lowering efficacy of bimatoprost and latanoprost in patients with ocular hypertension or glaucoma. *Am. J. Ophthalmol.* 135:55–63, 2003.
3. Parrish, R.K., Palmberg, P., and Sheu, W.P; XLT Study Group. A comparison of latanoprost, bimatoprost, and travoprost in patients with elevated intraocular pressure: a 12-week, randomized, masked-evaluator multicenter study. *Am. J. Ophthalmol.* 135:688–703, 2003.
4. Alm, A., and Stjernschantz, J. Effect of intraocular pressure and side effects of 0.005% latanoprost applied once daily, evening or morning. A comparison with timolol. Scandinavian Latanoprost Study Group. *Ophthalmology* 102:1743–1752, 1995.
5. Camras, C.B. Comparison of latanoprost and timolol in patients with ocular hypertension and glaucoma: a six-month masked, multicenter trial in the United States. The United States Latanoprost Study Group. *Ophthalmology* 103:138–147, 1996.
6. Watson, P., and Stjernschantz, J. A six-month, randomized, double-masked study comparing latanoprost with timolol in open angle glaucoma and ocular hypertension. The Latanoprost Study Group. *Ophthalmology* 103:126–137, 1996.
7. Woodward, D.F., Liang, Y., and Krauss, A.H. Prostamides (prostaglandin-ethanolamides) and their pharmacology. *Br. J. Pharmacol.* 153:410–419, 2008.
8. Woodward, D.F., Krauss, A.H.P., Chen, J., et al. The pharmacology of bimatoprost (Lumigan). *Surv. Ophthalmol.* 45(Suppl 4):S337–S345, 2001.
9. Brubaker, R.F., Schoff, E.O., Nau, C.B., et al. Effect of AGN 192024, a new ocular hypotensive agent, on aqueous dynamics. *Am. J. Ophthalmol.* 131:19–24, 2001.
10. Richter, M., Krauss, A.H., Woodward, D.F., and Lütjen-Drecoll, E. Morphological changes in the anterior eye segment after long-term treatment with different receptor selective prostaglandin agonists and a prostamide. *Invest. Ophthalmol. Vis. Sci.* 44:4419–4426, 2003.
11. Lim, K.S., Nau, C.B., O'Byrne, M.M., et al. Mechanism of action of bimatoprost, latanoprost, and travoprost in healthy subjects. A crossover study. *Ophthalmology* 115:790–795, 2008.
12. Christiansen, G.A., Nau, C.B., McLaren, J.W., and Johnson, D.H. Mechanism of ocular hypotensive action of bimatoprost (Lumigan) in patients with ocular hypertension or glaucoma. *Ophthalmology* 111:1658–1662, 2004.
13. Wan, Z., Woodward, D.F., Cornell, C.L., et al. Bimatoprost, prostamide activity, and conventional drainage. *Invest. Ophthalmol. Vis. Sci.* 48:4107–4115, 2007.
14. Gandolfi, S.A., and Cimino, L. Effect of bimatoprost on patients with primary open-angle glaucoma or ocular hypertension who are nonresponders to latanoprost. *Ophthalmology* 110;609–614, 2003.
15. Iwase, A., Suzuki, Y., Araie, M., et al.; Tajimi Study Group, Japan Glaucoma Society. The prevalence of primary open-angle glaucoma in Japanese: the Tajimi Study. *Ophthalmology* 111:1641–1648, 2004.
16. Yamamoto, T., Iwase, A., Araie, M., et al.; Tajimi Study Group, Japan Glaucoma Society. The Tajimi Study report 2: prevalence of primary angle closure and secondary glaucoma in a Japanese population. *Ophthalmology* 112:1661–1669, 2005.
17. Collaborative Normal-Tension Glaucoma Study Group. Comparison of glaucomatous progression between untreated patients with normal-tension glaucoma and patients with therapeutically reduced intraocular pressure. *Am. J. Ophthalmol.* 126:487–497, 1998.
18. Ikeda, Y., Mori, K., Ishibashi, T., et al. Latanoprost nonresponders with open-angle glaucoma in Japanese population. *Jpn. J. Ophthalmol.* 50:153–157, 2006.
19. Miyata, K., Amano, S., Sawa, M., and Nishida, T. A novel grading method for superficial punctate keratopathy magnitude and its correlation with corneal epithelial permeability. *Arch. Ophthalmol.* 121:1537–1539, 2003.
20. Rulo, A.H., Greve, E.L., Geijssen, H.C., and Hoyng PF. Reduction of intraocular pressure with treatment of latanoprost once daily in patients with normal-pressure glaucoma. *Ophthalmology* 103:1276–1282, 1996.
21. Cantor, L.B., Hoop, J., Wudunn, D., et al. Levels of bimatoprost acid in the aqueous humour after bimatoprost treatment of patients with cataract. *Br. J. Ophthalmol.* 91:629–632, 2007.
22. Woodward, D.F., Krauss, A.H., Chen, J., et al. Pharmacological characterization of a novel antiglaucoma agent, Bimatoprost (AGN 192024). *J. Pharmacol. Exp. Ther.* 305:772–785, 2003.
23. Sonty, S., Donthamsetti, V., Vangipuram, G., and Ahmad, A. Long-term IOP lowering with bimatoprost in open-angle glaucoma patients poorly responsive to latanoprost. *J. Ocul. Pharmacol. Ther.* 24:517–520, 2008.
24. Vielhauer, G.A., Fujino, H., and Regan, J.W. Cloning and localization of hFP(S): a six-transmembrane mRNA splice variant of the human FP prostanoid receptor. *Arch. Biochem. Biophys.* 15:175–185, 2004.
25. Liang, Y., Woodward, D.F., Guzman, V.M., et al. Identification and pharmacological characterization of the prostaglandin FP receptor and FP receptor variant complexes. *Br. J. Pharmacol.* 154:1079–1093, 2008.
26. Honrubia, F., García-Sánchez, J., Polo, V., Martínez de la Cass, J.M., and Soto, J. Conjunctival hyperemia with the use of latanoprost versus other prostaglandin analogues in patients with ocular hypertension or glaucoma: a meta-analysis of randomized clinical trials. *Br. J. Ophthalmol.* 93:316–321, 2009.
27. Kurtz, S., and Mann, O. Incidence of hyperemia associated with bimatoprost treatment in naïve subjects and in subjects previously treated with latanoprost. *Eur. J. Ophthalmol.* 19: 400–403, 2009.
28. Chen, J., Dinh, T., Woodward, D.F., et al. Bimatoprost: mechanism of ocular surface hyperemia associated with topical therapy. *Cardiovasc. Drug Rev.* 23:231–246, 2005.
29. Yam, J.C., Yuen, N.S., and Chan, C.W. Bilateral deepening of upper lid sulcus from topical bimatoprost therapy. *J. Ocul. Pharmacol. Ther.* 25:471–472, 2009.
30. Caprioli, J., and Coleman, A.L. Blood Flow in Glaucoma Discussion. Blood pressure, perfusion pressure, and glaucoma. *Am. J. Ophthalmol.* 149:704–712, 2010.
31. Quaranta, L., Pizzolante, T., Riva, I., Haidich, A.B., Konstas, A.G., and Stewart, W.C. Twenty-four-hour intraocular pressure and blood pressure levels with bimatoprost versus latanoprost in patients with normal-tension glaucoma. *Br. J. Ophthalmol.* 92:1227–1231, 2008.

Received: February 7, 2011
Accepted: June 27, 2011

Address correspondence to:
Dr. Kazuyuki Hirooka
Department of Ophthalmology
Kagawa University Faculty of Medicine
1750-1 Ikenobe
Miki, Kagawa 761-0793
Japan

E-mail: kazuyk@med.kagawa-u.ac.jp

厚生科学研究費補助金　障害者対策総合研究事業（感覚器障害分野）
分担研究報告書

未熟児網膜症の治療に使用する抗 VEGF 剤と無灌流領域

研究分担者　近藤　峰生　三重大学大学院医学系研究科神経感覚医学講座眼科学

研究要旨：未熟児網膜症（ROP）に対する新たな治療法として、抗 VEGF 剤の硝子体内注射が注目されている。これまでの報告では、抗 VEGF 剤の硝子体内注射は眼内新生血管の活動性を低下させることによって ROP の治療として有用であるとされている。しかし最近になり、抗 VEGF 剤の注射によって網膜での無灌流領域（NPA）が拡大するのではないかという報告がなされた。もしそうであれば、この治療法は ROP の治療薬として望ましくない一面があることになる。そこで今回我々は、網膜静脈分枝閉塞（BRVO）の患者 58 名 58 眼において抗 VEGF 剤であるベバシズマブ（アバスチン®）の硝子体内注射（IVB）と注射後 1 か月における NPA の面積を計測した。その結果、NPA の面積は IVB によって拡大していないことがわかった。今回の研究は ROP の網膜で計測したものではないが、少なくとも BRVO においては IVB は網膜の NPA を拡大させることはないことがわかった。

A．研究目的

血管内皮増殖因子（Vascular endothelial growth factor: VEGF）はROPにおける新生血管発生と増殖変化の主たる因子と考えられている。このVEGFを抑制する抗VEGF療法は、未熟児網膜症（ROP）に対する新たな治療法として注目されており、実際に良好な臨床成績が報告されてきている[参考文献1,2]。これまでの報告では、抗VEGF剤の硝子体内注射は眼内新生血管の活動性を低下させることによってROPの治療として有用であるとされている。

しかしながら最近になり、主に血管閉塞性疾患に使用した場合、抗VEGF剤の注射によって網膜での無灌流領域（NPA）が拡大するのではないかという報告がなされた [参考文献3-7]。もしそうであれば、この治療法はROPの治療薬として望ましくない一面があることになる。

そこで今回我々は、網膜静脈分枝閉塞（BRVO）の患者58名58眼において抗VEGF剤であるベバシズマブ（アバスチン®）の硝子体内注射（IVB）前と注射後1か月におけるNPAの面積を計測した。

B．研究方法

BRVOによる黄斑浮腫による治療目的でIVBを施行した58名58眼（男性25名、女性55名：年齢41-89歳、平均66.2歳）を対象とした。IVB施行前と施行後1か月の時点で蛍光眼底造影を施行し、NPAの面積をImageNet 1024®（Topcon）を使用して測定した。NPAの面積は、視神経乳頭の面積で除することによって乳頭面積（DA）で表した。出血によるブロックとNPAを鑑別するために、常に眼底写真と対比してNPAの領域のみを計測するようにした（図1）。

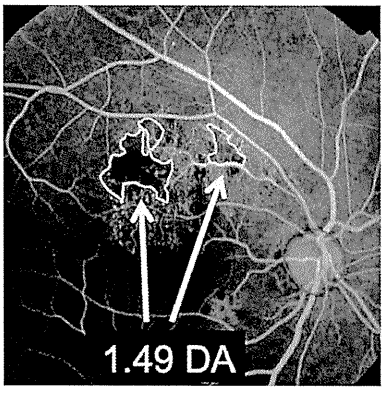

図1：NPAの計測方法。NPAの面積をデジタル計測し、乳頭面積で除してDAで表した。

（倫理面への配慮）

本研究は、名古屋大学医学部の倫理委員会の承認を得て行った。患者には今回の研究について十分説明の後に書面による承諾を得て行った。

C．研究結果

58眼中37眼はIVB前にNPAが存在しなかった。この37眼では、IVB後にNPAが出現したものが3眼あった。それらの面積は、0.13, 0.47, 0.60 DAであった。

58眼中21眼ではIVB前にNPAが存在しており、その面積は3.45±4.66 DAであった。これら21眼のIVB後1か月のNPA面積は、3.45±5.19 DAであった。両者には統計学的に有意な差はなかった（P=0.36）。

この21眼のIVB前後のNPA面積の変化を図2に示す。21眼で、IVB前後でNPA面積が1DA以上増加したものは1眼のみ（赤線）であった。一方で、IVB前後でNPA面積が1DA以上低下したものは4眼（青線）であった。

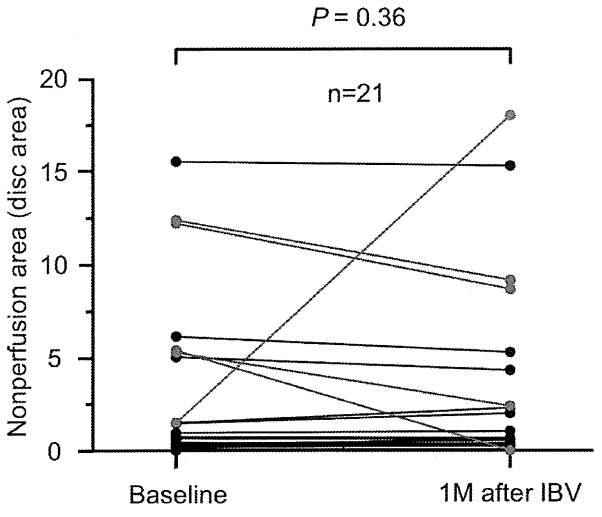

図2：BRVOでIVB施行前にNPAが存在した21眼におけるIVB前後のNPA面積の変化

図3にNPAがIVB前後に減少した症例の蛍光眼底造影検査の結果を示す。この症例は61歳の男性であり、NPA面積が12.4 DAから１か月の間に9.18 DAに減少した。

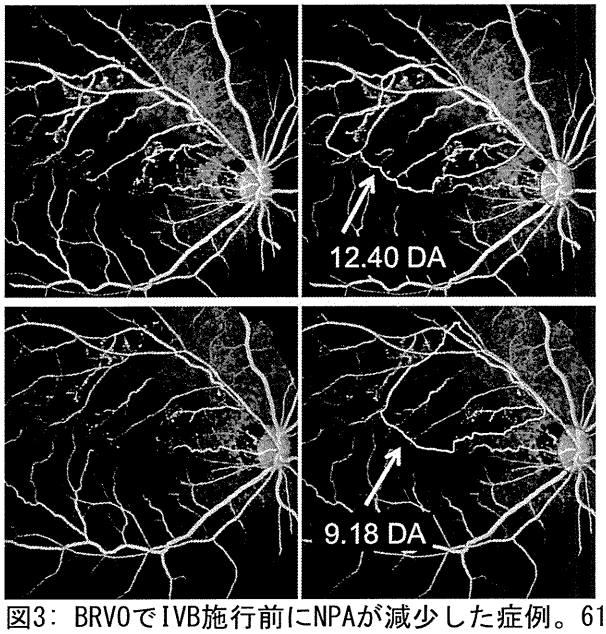

図3：BRVOでIVB施行前にNPAが減少した症例。61歳の男性で、NPA面積が12.4 DAから１か月の間に9.18 DAに減少した。

次に、図4にNPAがIVB前後で急激に増加した1眼（赤線）の蛍光眼底造影検査の結果を示す。この症例は67歳の女性であり、NPA面積が3.0 DAから18.0 DAに１か月の間に急激に増加した。

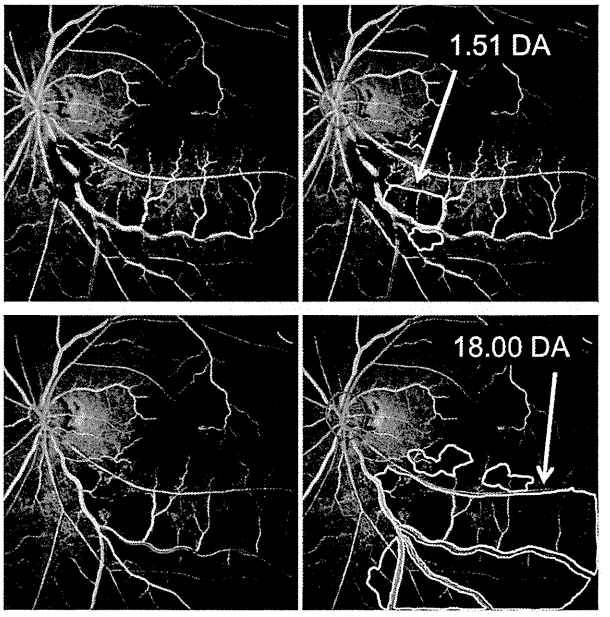

図4：BRVOでIVB施行前にNPAが増加した症例。67歳の女性で、NPA面積が1.51 DAから１か月の間に18.00 DAに増加した。

D．考察

最近になり、IVB後に網膜に虚血性変化が生じたという報告がいくつかみられる。Kimらは、CRVOの症例でIVB後に非虚血型が虚血型に変化した1例を報告している[参考文献6]。また、Papadopulouらは、抗VEGF剤注射後に網膜血管径が減少したことを報告している[参考文献4]。

その一方で、IVBは網膜における虚血性変化をおこさないという報告もある。CRVOとBRVOの29眼における定性的検討を行ったPragerらは、NPA面積はIVB前後で変化なかったと報告しているし、Kookらも糖尿病網膜症の129眼におけるNPAの検討により、その面積は増加していないことを報告している。

もしもIVBによって網膜に急激な虚血変化が引き起こされるのであれば、IVB後1か月の時点でNPAが増加する症例が多くみられるはずであると仮定して今回の研究を行った。その結果今回の我々のBRVO58眼の結果では、IVB前とIVB後で有意なNPA面積の変化はみられなかった。しかも、58眼中、IVB後にNPAが1DA以上増加したのはたったの1眼のみであった。以上により、IVBがNPAを促進させる可能性は低いと結論した。

それでは、なぜ我々の1眼で急激なNPAの増加がみられたのであろうか。Hayrehは、65歳以上のBRVOでは、発症から6か月の経過観察中に約16%の症例において、非虚血型から虚血型に移行することを報告している[参考文献7]。図3に示した症例は、そのような非虚血型から虚血型への移行症例であり、IVBとの関連で生じたものではなかっ

た可能性があると考えられた。

E．結論

今回の我々の研究結果により、少なくとも成人のBRVO症例においては、抗VEGF抗体の硝子体内注射は網膜のNPAを拡大させることはないということがわかった。しかしながら、今回の結果は実際のROPやROPモデル動物で行った実験ではない。ROPモデル動物を使った実験報告の中では完全なVEGFブロックは網膜の虚血性変化を促進させるという結果もあり、今後はさらに多くの疾患や動物実験による証拠の集積が必要であると考えられた。

F．健康危険情報

該当する危険あり（詳細）/なし

G．研究発表

1．論文発表

1) Terui T, Kondo M, et al. Changes in areas of capillary nonperfusion after intravitreal injection of bevacizumab in eyes with branch retinal vein occlusion. Retina. 2011;31:1068-1074.

2) Yasuda S, Kondo M, et al. Rebound of macular edema after intravitreal bevacizumab therapy in eyes with macular edema secondary to branch retinal vein occlusion. Retina. 2011;31:1075-1082.

3) Sanuki R, Onishi A, et al. miR-124a is required for hippocampal axogenesis and retinal cone survival through Lhx2 suppression. Nat Neurosci. 2011;14:1125-1134.

4) Kondo M, Sanuki R, et al. Identification of autoantibodies against TRPM1 in patients with paraneoplastic retinopathy associated with ON bipolar cell dysfunction. PLoS One. 2011;6:e19911.

5) Yasuda S, Kachi S, et al. Significant correlation between electroretinogram parameters and ocular vascular endothelial growth factor concentration in central retinal vein occlusion eyes. Invest Ophthalmol Vis Sci. 2011;52:5737-5742.

2．学会発表

1) Kondo M, Sanuki R, et al. Identification of autoantibodies against TRPM1 in patients with paraneoplastic retinopathy associated with ON bipolar cell dysfunction. Annual Meeting of the Association for Research in Vision & Ophthalmology. Fort Lauderdale. May 6. 2011.

2) Kondo M, Hirota R, et al. Photoreceptor and post-photoreceptoral contributions to photopic ERG a-wave in Rhodopsin P347L Transgenic Rabbits. International Society for Electrophysiology of Vision. Quebec. June 11, 2012.

H．知的財産権の出願・登録状況

なし

1．特許取得

なし

2．実用新案登録

なし

3．その他（参考文献）

1) Kusaka S et al. Efficacy of intravitreal injection of bevacizumab for severe retinopathy of prematurity: a pilot study. Br J Ophthalmol. 2008;92:1450-1455.

2) Mintz-Hittner HA et al. (BEAT-ROP Cooperative Group). Efficacy of intravitreal bevacizumab for stage 3+ retinopathy of prematurity. N Engl J Med. 2011;364:603-615.

3) Neubauer AS, et al. Bevacizumab and retinal ischemia. Ophthalmology 2007;114:2096.

4) Papadopoulou DN, et al. Intravitreal ranibizumab may induce retinal arteriolar vasoconstriction in patients with neovascular age-related macular degeneration. Ophthalmology 2009;116:1755–1761.

5) Ameri H, et al. The effects of intravitreous bevacizumab on retinal neovascular membrane and normal capillaries in rabbits. Invest Ophthalmol Vis Sci 2007;48:5708–5715.

6) Kim KS, et al. Ischaemic change after intravitreal bevacizumab (Avastin) injection for macular oedema secondary to non-ischaemic central retinal vein occlusion. Acta Ophthalmol 2008;86:925–927.

7) Sabet-Peyman EJ, et al. Progression of macular ischemia following intravitreal bevacizumab. Ophthalmic Surg Lasers Imaging 2009;40: 316–318.

8) Hayreh SS, et al. Incidence of various types of retinal vein occlusion and their recurrence and demographic characteristics. Am J Ophthalmol 1994;117:429–441.

Identification of Autoantibodies against TRPM1 in Patients with Paraneoplastic Retinopathy Associated with ON Bipolar Cell Dysfunction

Mineo Kondo[1*☯], Rikako Sanuki[2,3☯], Shinji Ueno[1], Yuji Nishizawa[4], Naozumi Hashimoto[5], Hiroshi Ohguro[6], Shuichi Yamamoto[7], Shigeki Machida[8], Hiroko Terasaki[1], Grazyna Adamus[9], Takahisa Furukawa[2,3*]

1 Department of Ophthalmology, Nagoya University Graduate School of Medicine, Nagoya, Aichi, Japan, **2** Department of Developmental Biology, Osaka Bioscience Institute, Suita, Osaka, Japan, **3** JST, CREST, Suita, Osaka, Japan, **4** Department of Biomedical Sciences, Chubu University, Kasugai, Aichi, Japan, **5** Department of Respiratory Medicine, Nagoya University Graduate School of Medicine, Nagoya, Aichi, Japan, **6** Department of Ophthalmology, Sapporo Medical University School of Medicine, Sapporo, Hokkaido, Japan, **7** Department of Ophthalmology and Visual Science, Chiba University Graduate School of Medicine, Chiba, Chiba, Japan, **8** Department of Ophthalmology, Iwate Medical University School of Medicine, Morioka, Iwate, Japan, **9** Department of Ophthalmology, Oregon Health and Science University, Portland, Oregon, United States of America

Abstract

Background: Paraneoplastic retinopathy (PR), including cancer-associated retinopathy (CAR) and melanoma-associated retinopathy (MAR), is a progressive retinal disease caused by antibodies generated against neoplasms not associated with the eye. While several autoantibodies against retinal antigens have been identified, there has been no known autoantibody reacting specifically against bipolar cell antigens in the sera of patients with PR. We previously reported that the transient receptor potential cation channel, subfamily M, member 1 (TRPM1) is specifically expressed in retinal ON bipolar cells and functions as a component of ON bipolar cell transduction channels. In addition, this and other groups have reported that human TRPM1 mutations are associated with the complete form of congenital stationary night blindness. The purpose of the current study is to investigate whether there are autoantibodies against TRPM1 in the sera of PR patients exhibiting ON bipolar cell dysfunction.

Methodology/Principal Findings: We performed Western blot analysis to identify an autoantibody against TRPM1 in the serum of a patient with lung CAR. The electroretinograms of this patient showed a severely reduced ON response with normal OFF response, indicating that the defect is in the signal transmission between photoreceptors and ON bipolar cells. We also investigated the sera of 26 patients with MAR for autoantibodies against TRPM1 because MAR patients are known to exhibit retinal ON bipolar cell dysfunction. Two of the patients were found to have autoantibodies against TRPM1 in their sera.

Conclusion/Significance: Our study reveals TRPM1 to be one of the autoantigens targeted by autoantibodies in at least some patients with CAR or MAR associated with retinal ON bipolar cell dysfunction.

Citation: Kondo M, Sanuki R, Ueno S, Nishizawa Y, Hashimoto N, et al. (2011) Identification of Autoantibodies against TRPM1 in Patients with Paraneoplastic Retinopathy Associated with ON Bipolar Cell Dysfunction. PLoS ONE 6(5): e19911. doi:10.1371/journal.pone.0019911

Editor: Steven Barnes, Dalhousie University, Canada

Received February 10, 2011; **Accepted** April 6, 2011; **Published** May 17, 2011

Funding: This work was supported by CREST from the Japan Science and Technology Agency (http://www.jst.go.jp/), and a Grant-in-Aid for Scientific Research (B)(C) (#20390448, #20390087, #20592075, #20791678) from the Ministry of Education, Culture, Sports, Science and Technology (http://www.jsps.go.jp/), the Takeda Science Foundation (http://www.takeda-sci.or.jp/), The Uehara Memorial Foundation (http://www.ueharazaidan.com/), the Naito Foundation (http://www.naito-f.or.jp/), the Novartis Foundation (#20-10, http://novartisfound.or.jp/), Mochida Memorial Foundation for Medical and Pharmaceutical Research (http://www.mochida.co.jp/zaidan/), the Senri Life Science Foundation (#S-2144, http://www.senri-life.or.jp/), the Kato Memorial Bioscience Foundation (http://www.katokinen.or.jp/) and the Japan National Society for the Prevention of Blindness (http://www.nichigan.or.jp/link/situmei.jsp). A grant from the National Institute of Health (E13053), was awarded to GA. The funders had no role in study design, data collection and analysis, decision to publish, or preparation of the manuscript.

Competing Interests: The authors have declared that no competing interests exist.

* E-mail: furukawa@obi.or.jp (TF); kondomi@med.nagoya-u.ac.jp (MK)

☯ These authors contributed equally to this work.

Introduction

Paraneoplastic retinopathy (PR) is a progressive retinal disorder caused by an autoimmune mechanism and is associated with the presence of anti-retinal antibodies in the serum generated against neoplasms not associated with the eye [1–4]. The retinopathy can develop either before or after the diagnosis of a neoplasm. Patients with PR can have night blindness, photopsia, ring scotoma, attenuated retinal arteriole, and abnormal electroretinograms (ERGs). The diagnosis of PR is usually made by the identification of neoplasms and anti-retinal autoantibodies in the sera.

PR includes two subgroups: cancer-associated retinopathy (CAR) [5,6] and melanoma-associated retinopathy (MAR) [7–10]. Although CAR and MAR share similar clinical symptoms, the ERG findings

are very different. Both a- and b-waves are severely attenuated in CAR, indicating extensive photoreceptor dysfunction, whereas only the b-wave is severely reduced while the a-wave is normal in MAR, suggesting bipolar cell dysfunction [8,9]. However, it was recently reported that cancers other than melanoma can cause bipolar cell dysfunction [11,12]. Several autoantibodies against retinal antigens have been identified, but a specific antigen associated with bipolar cells has not been identified in patients with CAR and MAR [1–10].

In the current study, we identified autoantibodies against the transient receptor potential cation channel, subfamily M, member 1 (TRPM1) [13–15] in the serum of one patient with lung cancer. The ERG findings in this patient indicated a selective ON-bipolar cell dysfunction. We also investigated the sera of 26 MAR patients and found that two contained autoantibodies against TRPM1. Our results suggest that TRPM1 is one of the retinal autoantigens in at least some patients with CAR or MAR and may cause retinal ON bipolar cell dysfunction.

Results

Case report of CAR associated with ON bipolar cell dysfunction

A 69-year-old man visited the Nagoya University Hospital with complaints of blurred vision, photopsia and night blindness in both eyes of three months duration. At this point he was not diagnosed as suffering from any eye disease or systemic disease, including a malignant tumor, and his family history revealed no other members suffering from any eye diseases. On initial examination, his best-corrected visual acuity was 0.9 in the right eye and 0.6 in the left eye. Humphrey static perimetry revealed a severe decrease in sensitivity within the central 30 degrees of the visual field in both eyes (Fig. 1A). Dark-adaptometry of this patient showed a loss of the rod branch. The cone threshold was within normal range. Ophthalmoscopy showed a nearly normal fundus appearance except for slight hypopigmentation at the macula of the left eye, which may be due to age-related changes in the retinal pigment epithelium (Fig. 1B), but fluorescein angiography demonstrated periphlebitis of the retinal vessels (arrows, Fig. 1C). Spectral-domain optical coherence tomography (SD-OCT) showed that the morphology of the retina was normal in both eyes (Fig. 1D).

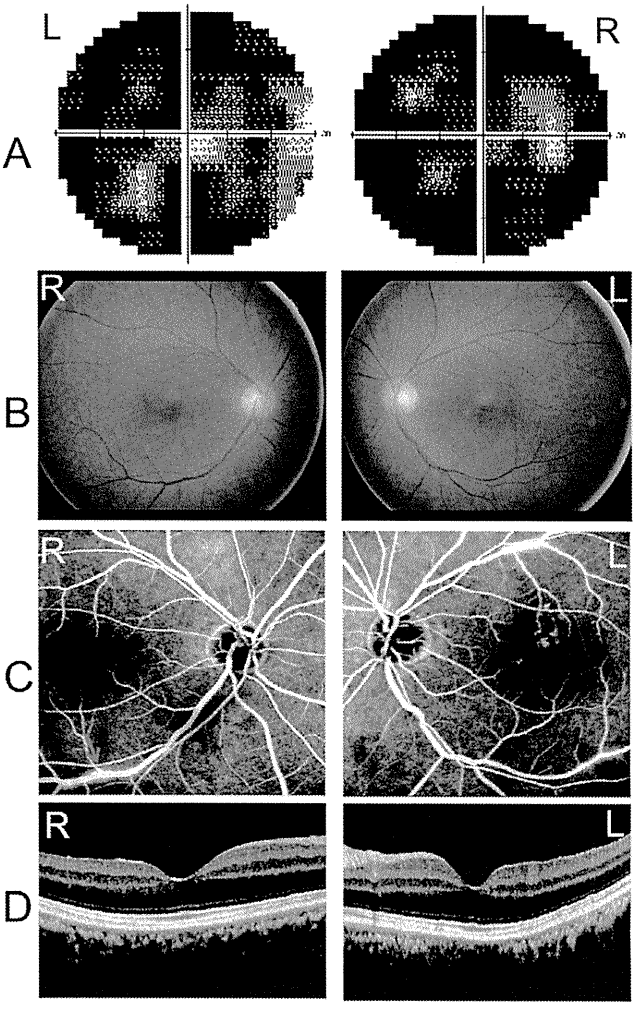

Figure 1. Ophthalmological findings from a patient with paraneoplastic retinopathy (PR) associated with lung cancer. (A) Threshold of static visual field (Humphrey, 30-2 program) plotted on a gray scale showing severely decreased sensitivities within the central 30 degrees of the visual field. (B) Fundus photographs of the patient showing a nearly normal fundus. (C) Fluorescein angiograms showing periphlebitis of the retinal vessels (arrows). (D) Spectral-domain optical coherence tomographic (SD-OCT) image of a 9 mm horizontal scan of the retina of our patient. The retinal structure in each retinal layer is normal.
doi:10.1371/journal.pone.0019911.g001

Electrophysiological examinations

Recordings of the full-field ERGs from this patient showed that the rod responses were undetectable (Fig. 2). The rod- and cone-mixed maximal response was a negative-type with an a-wave of normal amplitude and a b-wave that was smaller than the a-wave. The a-wave of the cone response had a wide trough, and the b-wave was reduced by 40%. The amplitude of the 30-Hz flicker ERG was reduced by 50%. The photopic long-flash ERG showed severely reduced ON response and normal OFF response. These ERG findings indicated that there was a defect in the signal transmission from photoreceptors to ON bipolar cells both in both rod and cone pathways.

Based on these ophthalmological and electrophysiological tests, we suspected that this patient might have PR and referred him to an internist. The general physical examination including positron emission tomography and computed tomography revealed two abnormal masses in the right lung. Biopsy of these masses confirmed that the masses were small cell carcinomas of the lung.

Detection of autoantibodies against TRPM1 in the serum of the CAR patient

Based on our ERG examination results, we hypothesized that the serum of this CAR patient may contain autoantibodies against TRPM1. To test this hypothesis, we examined whether or not this CAR patient's serum could recognize human TRPM1 protein by Western blot analysis. We transfected an expression plasmid containing human TRPM1 cDNA with the C-terminal 3xFlag-tag (TRPM1-3xFlag) into HEK293T cells, and carried out a Western blot analysis using whole cell extracts harvested after 48 hrs cell growth. We first confirmed that TRPM1-3xFlag was expressed by cell using Western blot analysis and an anti-Flag antibody. We detected the ~200 kDa TRPM1-3xFlag band in the cell lysates (Fig. 3A).

Next, we performed Western blot analysis on the same lysates using the serum from our CAR patient and a healthy control person. We detected immunostaining of the same size protein, which was confirmed with the anti-Flag antibody, and with CAR serum. The control serum did not present a significant band (Fig. 3B, C). This result showed the presence of autoantibodies against TRPM1 in this CAR patient's serum.

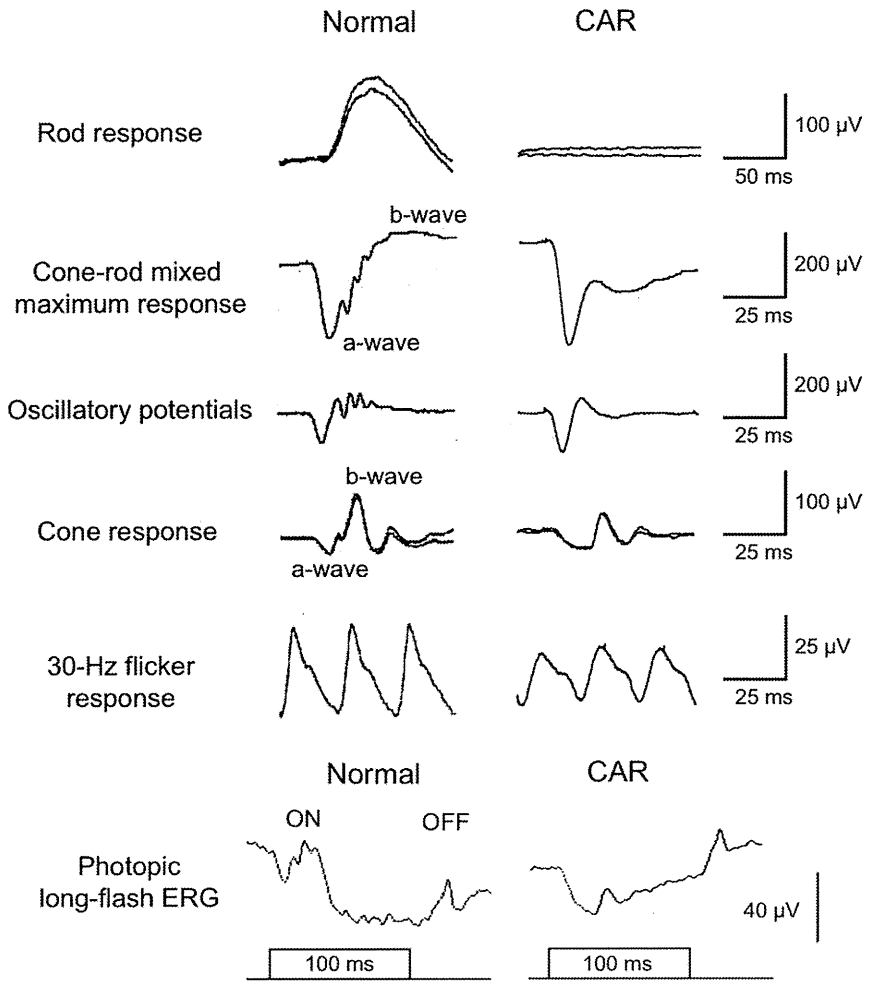

Figure 2. Full-field ERG recordings. The rod response was recorded with a blue light at an intensity of 5.2×10^{-3} cd-s/m^2 after 30 minutes of dark-adaptation. The cone-rod mixed maximum response was elicited by a white flash at an intensity of 44.2 cd-s/m^2. The oscillatory potentials were recorded with a white flash at an intensity of 44.2 cd-s/m^2 using a band-pass filter of 50–1000 Hz. The cone response and a 30 Hz flicker response were elicited by a white stimulus of 4 cd-s/m^2 and 0.9 cd-s/m^2, respectively, on a blue background of 30 cd/m^2. Photopic long-flash ERG responses were also elicited by long-duration flashes of 100 ms using a densely-packed array of white LEDs of 200 cd/m^2 on a white background of 30 cd/m^2.
doi:10.1371/journal.pone.0019911.g002

To examine whether the serum from the CAR patient recognized retinal bipolar cells, we carried out an immunohistochemical analysis on monkey and mouse retinas. We first performed immunohistochemistry on the retina of a 3-year-old rhesus monkey (*Macaca mulata*) and on the retina of a one-month-old C57/B6 mouse using the serum of the CAR patient, however, we did not obtain a significant staining signal above background (data not shown). We then concentrated the serum by IgG purification followed by filter spin column centrifugation and performed immunohistochemistry on the monkey retina using the concentrated serum (Fig. 3D–G). We observed a significant immunolabeling on the INL in the monkey retina (Fig. 3D, F) whereas the normal serum did not give a significant labeling (Fig. 3E, G). The antibodies immuolabeled both the bipolar side and amacrine side of the INL. Since most of the cells residing on the outer side of the INL are ON bipolar cells, at least some of the stained cells are ON bipolar cells. It should be noted some of the staining signals show a spotted pattern in the outer plexiform layer (Fig. 3F) as is observed in TRPM1 or mGluR6 immunostaining on the mouse retina [13], suggesting that the CAR patient serum recognizes the bipolar dendritic tips where some of the TRPM1 protein localizes.

Western blot analysis of the sera from MAR patients

Since the functional defect in the retina of MAR patients is known to be due to abnormal signal transmission between photoreceptors and ON bipolar cells [8,9], we then investigated whether or not autoantibodies to TRPM1 were also present in the sera of MAR patients. We obtained the sera of 26 MAR patients from two hospitals in Japan (Chiba University Hospital and Iwate Medical University Hospital) and Ocular Immunology Laboratory in the USA (Casey Eye Institute). We found that the sera from patients #8 and #23 exhibited a significant immunoreactive band against TRPM1-transfected cell lysates by Western blot analysis (Fig. 4A and B). The control serum showed no significant immune response against the TRPM1-transfected cell lysates (Fig. 3C). These results suggest that the sera from some MAR patients contain autoantibodies against TRPM1. Due to the limited volume of sera from the MAR patients, we could not try immunostaining on the monkey or the mouse retina using the serum from the patients #8 and #23.

MAR patient #8, was a 76-year-old man with a history of skin melanoma. He had ring scotomas and abnormal ERGs indicating that he had MAR. The other patient, MAR #23, was a 57-year-

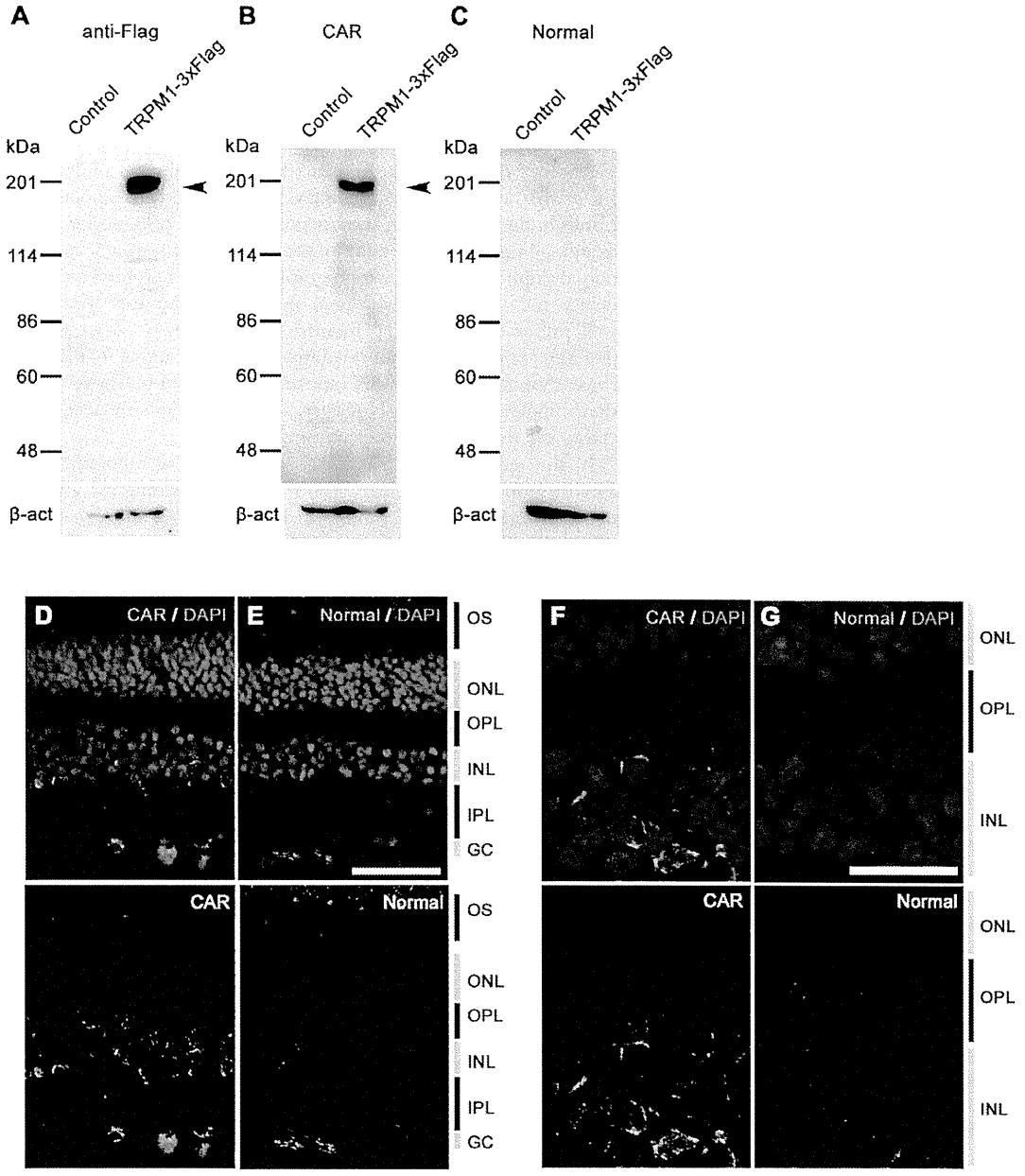

Figure 3. Immunostaining and Western blot analysis of human TRPM1 using serum from the CAR patient. (A–C) Immunoblots of the transfected cell lysates using an antibody against Flag tag (A), serum from CAR patient (B), and control serum (C). Arrowheads indicate the TRPM1-3xFlag protein bands. HEK293T cells were transfected with the pCAGGS or pCAGGS-human TRPM1-3xFlag plasmid, and cells were harvested after 48 hrs. β-actin (β-act) was used for a loading control. (D–G) Confocal images of a three-year-old rhesus monkey retina immunostained with the concentrated serum from the CAR patient (D, F) or the concentrated normal serum (E, G). Cell nuclei are visualized with DAPI. CAR patient serum presented signals on INL cells and the inner part of the OPL (D, F). Scale bar = 50 μm in (E) and 20 μm in (G).
doi:10.1371/journal.pone.0019911.g003

old man with poor night vision, abnormal scotopic ERGs and abnormal color vision. He had a history of skin melanoma and thyroid cancer. There was no other clinical information available on these two patients because these sera were obtained from other institutes several years before without detailed clinical information.

Discussion

PR, including MAR and CAR, presents visual disorders associated with systemic cancer. Antibodies against retinal cells and proteins have been detected in the sera of patients with PR suggesting an autoimmune basis for the etiology of the PR. The autoantibodies identified so far include rhodopsin, retinal transducin alpha and beta, recoverin, S-arrestin, α-enolase, carbonic anhydrase II, and heat shock protein-60 which reside abundantly in photoreceptors [1–10,16]. MAR and CAR can cause bipolar cell dysfunction [7–12]. The results of the ERG [8,9] and immunohistochemistry [7] studies suggested that the main target of MAR are retinal ON bipolar cells in both the rod and cone pathways. However, autoantibodies specifically reacting with a bipolar cell antigen had not been identified in the sera of patients with PR, including those with CAR and MAR. In the current study, we identified autoantibodies against TRPM1, a component of the ON bipolar cell transduction channel negatively regulated by Goα in the mGluR6 signaling pathway [13–15], in the

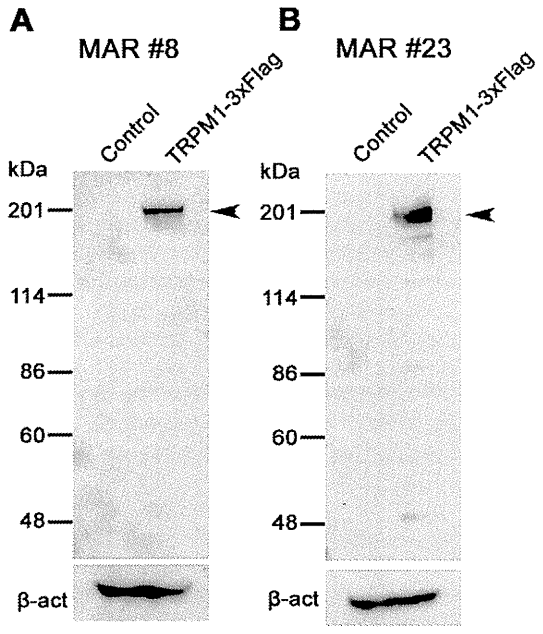

Figure 4. Western blot analysis of human TRPM1 using sera from the MAR patients. (A, B) Immunoblots of the transfected cell lysates using sera from MAR patient #8 (A) and MAR patient #23 (B). HEK293T cells were transfected with pCAGGS or pCAGGS-human TRPM1-3xFlag plasmid, and cells were harvested after 48 hrs. Arrowheads indicate the TRPM1-3xFlag protein bands. β-actin (β-act) was used for a loading control.
doi:10.1371/journal.pone.0019911.g004

sera of one CAR patient and two MAR patients. The CAR patient exhibited a dysfunction of ON bipolar cells, and to our knowledge, this is the first report on an autoantibody against a bipolar cell antigen in the serum of PR patients affecting the ON bipolar cell function.

Previously, we isolated a mouse *TRPM1-L* cDNA corresponding to the human long form of *TRPM1*, and found that the TRPM1-L protein is developmentally localized at the tips of the ON bipolar dendrites co-localizing with mGluR6, but not on OFF bipolar cells [13,14]. The *TRPM1* null mutant mouse completely loses the ON bipolar cell photoresponses to light, indicating that TRPM1 plays a critical role in the synaptic transmission from photoreceptors to ON-bipolar cells [13,15]. In addition, we demonstrated using a CHO cell reconstitution system that TRPM1-L is a nonselective cation channel which is negatively regulated by Goα downstream of the mGluR6 signaling cascade in ON bipolar cells [13]. Recently, four groups including ours independently reported that mutations of human *TRPM1* are associated with the complete-type of congenital stationary night blindness (cCSNB), an inherited human retinal disease [17–20]. cCSNB is a non-progressive retinal disease characterized by congenital night blindness with a moderate decrease in visual acuity and myopia [21-24]. Previous ERG studies have suggested that the defect in cCSNB patients lies in the signal transmission from photoreceptors to ON bipolar cells in both the rod and cone pathways [25–28]. We have identified five different mutations in our three cCSNB patients, and have shown that these mutations lead to either abnormal TRPM1 protein production or mislocalization of the TRPM1 protein in bipolar cell dendrites [17]. These results suggest that TRPM1 plays a critical role in mediating the photoresponses of ON bipolar cells in humans as well. Based on these findings, we hypothesize that the ectopic expression of TRPM1 in tumor cells of some CAR and MAR patients may result in aberrant production of autoantibodies to TRPM1 through B-lymphocytic responses [29–32]. These antibodies may react to the TRPM1 protein in retinal ON bipolar cells resulting in dysfunction of the TRPM1 transduction cation channel downstream of the mGluR6 signaling cascade. However, we could not confirm whether TRPM1 is expressed in the tumor cells of the three PR patients examined in this study [29] because tumor samples were not available.

Another question regarding the disease mechanism underlying PR is whether the binding of TRPM1 autoantibody to bipolar cells results in the cell death or dysfunction of bipolar cells. As far as we examined the retinal structure of the CAR patient using a spectral domain optical coherence tomography (SD-OCT) retinal imaging device, the structure of the retinal bipolar cell layer appeared to be well preserved even three months after the onset of symptoms (Fig.1D). This suggests that the autoantibodies reacting to TRPM1 cause dysfunction of the ON bipolar transduction pathway rather than bipolar cell death. However, further studies are needed to clarify the exact disease mechanism.

In the sera of MAR patients, several types of autoantibodies against retinal proteins have been reported, including the 22 kDa neuronal antigen GNB1, rhodopsin, S-arrestin, and aldolase-A and -C [10,16,33,34]. We initially considered that TRPM1 might be a major MAR target antigen, because TRPM1 is exclusively expressed in retinal ON bipolar cells. However, autoantibodies against TRPM1 were detected in only two out of 26 MAR. patients' sera (7.7%, Fig. 4A, B). We tested whether the sera of one CAR patient and 26 MAR patients recognized human mGluR6, which is specifically expressed in ON bipolar cells, however, none of the sera exhibited a significant band in Western blot analysis (data not shown). Thus, antigens other than TRPM1 or mGluR6 may be involved in the pathogenesis of a large proportion of MAR.

Immunohistochemical analyses using the serum of the CAR patient showed labeling in the inner nuclear layer and outer plexiform layer of the adult rhesus monkey retina (Fig. 3D–G), where the bipolar cell bodies and dendrites reside, respectively. This immunostaining pattern is somewhat similar to our previous immunostaining results on the mouse retina with specific antibody against mouse TRPM1-L, which corresponds to the human TRPM1 long form [13]. Other labeling was also observed in the amacrine cells and ganglion cells. The reason for the immunoreactivity with these cells is uncertain, however, it may be due to the presence of other autoantibodies against amacrine cell and ganglion cell antigens. Lu *et al.* reported the presence of various different autoantibodies in the serum of a single PR patient [10]. If this is the case, it may explain why our CAR patient displayed severely reduced visual sensitivities in the visual field tests (Fig. 1A) unlike cCSNB patients with TRPM1 mutations[17].

It should be noted that we did not confirm whether there are any antoantibodies against TRPM1 in the sera of normal subjects by using a large number of samples. However, this possibility is thought to be low, because Shimazaki *et al.* reported that the molecular weights of the IgGs with observed anti-retinal reactivity in 92 normal sera were smaller than 148 kDa, which is smaller than the TRPM1 molecular weight of ~200 kDa, although relatively high molecular weight reactivity was not intensively investigated [35].

One limitation of the current study is that we could not obtain detailed information on the two MAR patients, MAR #8 and #23, associated with the TRPM1 autoantibody. We confirmed that these two patients had skin melanomas accompanying the visual disturbances, but could not obtain a more detailed clinical history or data on visual acuity, visual field, or ERGs because these sera were sent from different hospitals several years ago. Thus, we do not know whether these two MAR patients really had retinal ON bipolar cell dysfunction. Further prospective studies of the TRPM1 autoantibodies in large numbers of MAR patients are needed.

In conclusion, our study suggests that TRPM1 may be one of the causative antigens responsible for PR associated with ON bipolar cell dysfunction.

Note added in proof

During the course of revision process of this manuscript, Dhingra *et al.* (J. Neurosci. 31, 3962–3967, 2011) independently reported the presence of autoantibodies against TRPM1 in two MAR patients. Our study reports on autoantibodies against TRPM1 in CAR serum in addition to MAR sera.

Materials and Methods

Subjects

The Nagoya University Hospital Ethics Review Board approved this study (approval ID 1131). Of the PR patients that were examined in the Nagoya University Hospital, one PR patient with lung cancer and ON bipolar cell dysfunction was studied in detail. The examinations included routine ophthalmological and electrophysiological tests. In addition, immunohistochemical and Western blot analyses were performed using the serum of this patient. The procedures used conformed to the tenets of the Declaration of Helsinki of the World Medical Association. A written informed consent was obtained from the patient after he was provided with sufficient information on the procedures to be used.

We also obtained sera of 26 patients with MAR from two hospitals in Japan (Chiba University Hospital and Iwate Medical University Hospital) and Ocular Immunology Laboratory in the USA (Casey Eye Institute) for Western blot analysis.

Ophthalmologic examinations

The ophthalmologic examination included best-corrected visual acuity, biomicroscopy, ophthalmoscopy, fundus photography, fluorescein angiography, static perimetry, and spectral-domain optical coherence tomography (SD-OCT). Static visual fields were obtained with the Humphrey 30-2 program (Carl Zeiss, Dublin, USA), and the results are shown in gray scale. SD-OCT was performed with a 9-mm horizontal scan through the midline with 50 averages (Spectralis HRA+OCT; Heidelberg Engineering, Vista, CA).

Electroretinograms (ERG)

Full-field ERGs were elicited with a Ganzfeld dome and recorded with a Burian-Allen bipolar contact lens electrode. The ground electrode was attached to the ipsilateral ear.

After 30 minutes of dark-adaptation, a rod response was elicited with a blue light at an intensity of 5.2×10^{-3} cd-s/m^2. A cone-rod mixed maximum response was elicited by a white flash at an intensity of 44.2 cd-s/m^2. A cone response and a 30 Hz flicker response were elicited by a white stimulus of 4 cd-s/m^2 and 0.9 cd-s/m^2, respectively, on a blue background of 30 cd/m^2. Full-field cone ERGs were also elicited by long-duration flashes of 100 ms using a densely packed array of white LEDs. The array was positioned at the top of the Ganzfeld dome and covered by a diffuser. The stimulus intensity and background illumination measured in the dome was 200 cd/m^2 and 30 cd/m^2, respectively. Responses were amplified by 10K and the band pass was set to 0.3 to 1000 Hz. The data were digitized at 4.3 kHz, and 5 to 20 responses were averaged (Neuropack, Nihonkohden, Tokyo, Japan).

Immunohistochemistry

For immunohistochemistry, patient and normal sera (300 µl) were purified using the Melon Gel IgG purification kit according to the manufacturer's protocol (Pierce Biotechnology, Rockford, IL) to remove IgM, and purified sera were concentrated by Amicon Ultra 100 (Millipore, MA). The rhesus monkey eye cup was fixed with 4% paraformaldehyde in PBS for 30 min at 4°C. The samples were cryoprotected with 30% sucrose in PBS and embedded in OCT compound (Sakura Finetechnical, Tokyo, Japan). These tissues were sliced with a Microm HM 560 cryostat microtome (Microm Laborgeräte GmbH, Walldorf, Germany) into 14 µm. Sections were washed twice in PBS for 5 min, permeabilized with 0.1% Triton-X100/PBS, then washed with PBS 3 times for 5 min, and incubated with PBS containing 4% donkey serum for 1 hr to block samples. For the immunoreaction, the samples were incubated with a purified normal or CAR serum (1:300) diluted in blocking buffer at 4°C overnight. After PBS-washing, these samples were incubated with a DyLight-488 conjugated donkey anti-human IgG (H+L) (1:400) as a secondary antibody (Jackson Immunoresearch Laboratories) at room temperature for 1 hr and washed with PBS.

Transfection and Western blot analyses

HEK293T cells were cultured in D-MEM containing 10% fetal bovine serum (FBS; Nissui, Tokyo, Japan). These cells were grown under 5% carbon dioxide at 37°C. The calcium phosphate method was used to transfect the cells. Transfected cells were incubated at 37°C for 48 hrs, and then harvested for further analysis. The proteins extracted from the cells were separated by SDS–PAGE on a 7.5% precast gel (ATTO, Tokyo, Japan), and then transferred to a polyvinylidene difluoride membrane using the Invitrogen iBlot system (Invitrogen, Carlsbad, CA, USA). The membrane was incubated with primary antibodies, mouse anti-Flag (1:1,000; Sigma, St Louis, MO), sera from patients (1:100), normal human serum (1:100), or mouse anti-β-actin (1:5,000; Sigma). The membrane was then incubated with a horseradish peroxidase-conjugated goat anti-mouse IgG (1:10,000; Zymed Laboratories, San Francisco, CA) or donkey anti-human IgG (1:10,000; Jackson Immuno Research Laboratories, West Grove, PA) as secondary antibodies. The bands were developed using Chemi-Lumi One L (Nacalai Tesque, Kyoto, Japan).

Acknowledgments

We thank Richaed G. Weleber, Yozo Miyake, and Duco I. Hamasaki for helpful discussions of this study, Junko Hanaya for collecting the serum of our patients, and Mikiko Kadowaki, Aiko Ishimaru, Kaori Sone, and Shawna Kennedy for technical assistance.

Author Contributions

Conceived and designed the experiments: MK TF. Performed the experiments: MK RS SU YN NH. Analyzed the data: MK RS SU TF. Contributed reagents/materials/analysis tools: MK SU HO SY SM HT GA. Wrote the paper: MK TF. Supervised the project: MK HT TF.

References

1. Thirkill CE, FitzGerald P, Sergott RC, Roth AM, Tyler NK, et al. (1989) Cancer-associated retinopathy (CAR syndrome) with antibodies reacting with retinal, optic-nerve, and cancer cells. N Engl J Med 321: 1589–1594.
2. Chan JW (2003) Paraneoplastic retinopathies and optic neuropathies. Surv Ophthalmol 48: 12–38.
3. Heckenlively JR, Ferreyra HA (2008) Autoimmune retinopathy: A review and summary. Semin Immunopathol 30: 127–134.
4. Adamus G (2009) Autoantibody targets and their cancer relationship in the pathogenicity of paraneoplastic retinopathy. Autoimmun Rev 8: 410–414.

5. Thirkill CE, Roth AM, Keltner JL (1987) Cancer-associated retinopathy. Arch Ophthalmol 105: 372–375.
6. Jacobson DM, Thirkill CE, Tipping SJ (1990) A clinical triad to diagnose paraneoplastic retinopathy. Ann Neurol 28: 162–167.
7. Milam AH, Saari JC, Jacobson SG, Lubinski WP, Feun LG, et al. (1993) Autoantibodies against retinal bipolar cells in cutaneous melanoma-associated retinopathy. Invest Ophthalmol Vis Sci 34: 91–100.
8. Alexander KR, Fishman GA, Peachey NS, Marchese AL, Tso MOM (1992) "On" response defect in paraneoplastic night blindness with cutaneous malignant melanoma. Invest Ophthalmol Vis Sci 33: 477–483.
9. Lei B, Bush RA, Milam AH, Sieving PA (2000) Human melanoma-associated retinopathy (MAR) antibodies alter the retinal ON-response of the monkey ERG in vivo. Invest Ophthalmol Vis Sci 41: 262–266.
10. Lu Y, Jia L, He S, Hurley MC, Leys MJ, et al. (2009) Melanoma-associated retinopathy: a paraneoplastic autoimmune complication. Arch Ophthalmol 127: 1572–1580.
11. Jacobson DM, Adamus G (2001) Retinal anti-bipolar cell antibodies in a patient with paraneoplastic retinopathy and colon carcinoma. Am J Ophthalmol 131: 806–808.
12. Goetgebuer G, Kestelyn-Stevens AM, De Laey JJ, Kestelyn P, Leroy BP (2008) Cancer-associated retinopathy (CAR) with electronegative ERG: a case report. Doc Ophthalmol 116: 49–55.
13. Koike C, Obara T, Uriu Y, Numata T, Sanuki R, et al. (2010) TRPM1 is a component of the retinal ON bipolar cell transduction channel in the mGluR6 cascade. Proc Natl Acad Sci U S A 107: 332–337. Epub Dec. 4, 2009.
14. Koike C, Numata T, Ueda H, Mori Y, Furukawa T (2010) TRPM1: A vertebrate TRP channel responsible for retinal ON bipolar function. Cell Calcium 48: 95–101.
15. Morgans CW, Zhang J, Jeffrey BG, Nelson SM, Burke NS, et al. (2009) TRPM1 is required for the depolarizing light response in retinal ON-bipolar cells. Proc Natl Acad Sci U S A 106: 19174–19178.
16. Hartmann TB, Bazhin AV, Schadendorf D, Eichmüller SB (2005) SEREX identification of new tumor antigens linked to melanoma-associated retinopathy. Int J Cancer 114: 88–93.
17. Nakamura M, Sanuki R, Yasuma TR, Onishi A, Nishiguchi KM, et al. (2010) TRPM1 mutations are associated with the complete form of congenital stationary night blindness. Mol Vis 16: 425–437.
18. Li Z, Sergouniotis PI, Michaelides M, Mackay DS, Wright GA, et al. (2009) Recessive mutations of the gene TRPM1 abrogate ON bipolar cell function and cause complete congenital stationary night blindness in humans. Am J Hum Genet 85: 711–719.
19. van Genderen MM, Bijveld MM, Claassen YB, Florijn RJ, Pearring JN, et al. (2009) Mutations in TRPM1 are a common cause of complete congenital stationary night blindness. Am J Hum Genet 85: 730–736.
20. Audo I, Kohl S, Leroy BP, Munier FL, Guillonneau X, et al. (2009) TRPM1 is mutated in patients with autosomal-recessive complete congenital stationary night blindness. Am J Hum Genet 85: 720–729.
21. Miyake Y, Yagasaki K, Horiguchi M, Kawase Y, Kanda T (1986) Congenital stationary night blindness with negative electroretinogram: A new classification. Arch Ophthalmol 104: 1013–1020.
22. Bech-Hansen NT, Naylor MJ, Maybaum TA, Sparkes RL, Koop B, et al. (2000) Mutations in NYX, encoding the leucine-rich proteoglycan nyctalopin, cause X-linked complete congenital stationary night blindness. Nat Genet 26: 319–23.
23. Pusch CM, Zeitz C, Brandau O, Pesch K, Achatz H, et al. (2000) The complete form of X-linked congenital stationary night blindness is caused by mutations in a gene encoding a leucine-rich repeat protein. Nat Genet 26: 324–327.
24. Dryja TP, McGee TL, Berson EL, Fishman GA, Sandberg MA, et al. (2005) Night blindness and abnormal cone electroretinogram ON responses in patients with mutations in the GRM6 gene encoding mGluR6. Proc Natl Acad Sci USA 102: 4884–4889.
25. Miyake Y, Yagasaki K, Horiguchi M, Kawase Y (1987) On- and off-responses in photopic electroretinogram in complete and incomplete types of congenital stationary night blindness. Jpn J Ophthalmol 31: 81–87.
26. Houchin K, Purple RL, Wirtschafter JD (1991) X-linked congenital stationary night blindness and depolarizing bipolar system dysfunction. [ARVO abstract]. Invest Ophthalml Vis Sci 32: S1229.
27. Young RSL (1991) Low-frequency component of the photopic ERG in patients with X-linked congenital stationary night blindness. Clin Vis Sci 6: 309–315.
28. Khan NW, Kondo M, Hiriyanna KT, Jamison JA, Bush RA, et al. (2005) Primate retinal signaling pathways: Suppressing ON-pathway activity in monkey with glutamate analogues mimics human CSNB1-NYX genetic night blindness. J Neurophysiol 93: 481–492.
29. Polans AS, Witkowska D, Haley TL, Amundson D, Baizer L, et al. (1995) Recoverin, a photoreceptor-specific calcium-binding protein, is expressed by the tumor of a patient with cancer-associated retinopathy. Proc Natl Acad Sci U S A 92: 9176–9180.
30. Matsubara S, Yamaji Y, Sato M, Fujita J, Takahara J (1996) Expression of a photoreceptor protein, recoverin, as a cancer-associated retinopathy autoantigen in human lung cancer cell lines. Br J Cancer 74: 1419–1422.
31. Ohguro H, Odagiri H, Miyagawa Y, Ohguro I, Sasaki M, et al. (2004) Clinicopathological features of gastric cancer cases and aberrantly expressed recoverin. Tohoku J Exp Med 202: 213–219.
32. Bazhin AV, Schadendorf D, Willner N, De Smet C, Heinzelmann A, et al. (2007) Photoreceptor proteins as cancer-retina antigens. Int J Cancer 120: 1268–76.
33. Keltner JL, Thirkill CE (1999) The 22-kDa antigen in optic nerve and retinal diseases. J Neuroophthalmol 19: 71–83.
34. Potter MJ, Adamus G, Szabo SM, Lee R, Mohaseb K, et al. (2002) Autoantibodies to transducin in a patient with melanoma-associated retinopathy. Am J Ophthalmol 134: 128–30.
35. Shimazaki K, Jirawuthiworavong GV, Heckenlively JR, Gordon LK (2008) Frequency of anti-retinal antibodies in normal human serum. J Neuro-Ophthalmol 28: 5–11.

miR-124a is required for hippocampal axogenesis and retinal cone survival through Lhx2 suppression

Rikako Sanuki[1,2], Akishi Onishi[1,2], Chieko Koike[1], Rieko Muramatsu[3], Satoshi Watanabe[1,2], Yuki Muranishi[1], Shoichi Irie[1,2], Shinji Uneo[4], Toshiyuki Koyasu[4], Ryosuke Matsui[5], Yoan Chérasse[6], Yoshihiro Urade[6], Dai Watanabe[5], Mineo Kondo[4], Toshihide Yamashita[3] & Takahisa Furukawa[1,2]

MicroRNA-124a (miR-124a) is the most abundant microRNA expressed in the vertebrate CNS. Despite past investigations into the role of miR-124a, inconsistent results have left the *in vivo* function of miR-124a unclear. We examined the *in vivo* function of miR-124a by targeted disruption of *Rncr3* (*retinal non-coding RNA 3*), the dominant source of miR-124a. *Rncr3*$^{-/-}$ mice exhibited abnormalities in the CNS, including small brain size, axonal mis-sprouting of dentate gyrus granule cells and retinal cone cell death. We found that *Lhx2* is an *in vivo* target mRNA of miR-124a. We also observed that LHX2 downregulation by miR-124a is required for the prevention of apoptosis in the developing retina and proper axonal development of hippocampal neurons. These results suggest that miR-124a is essential for the maturation and survival of dentate gyrus neurons and retinal cones, as it represses *Lhx2* translation.

MicroRNAs (miRNAs) are small RNAs that regulate gene expression by base-pairing to mRNAs. Notably, miR-124a is completely conserved at the nucleotide level from worms to humans and is estimated to be the most abundant miRNA in the brain, accounting for 25–48% of all brain miRNAs[1]. In addition, the human miR-124a-1 locus is located in the chromosome 8p23 region, which is rich in genes that have been implicated in neuropsychiatric disorders, microcephaly and epilepsy[2]. Overexpression of miR-124a in HeLa cells leads to the suppression of a large number of non-neuronal transcripts[3]. Moreover, a neurogenesis suppressor gene, *Ctdsp1*, and a neuron-specific splicing repressor gene, *Ptbp1*, have been identified as miR-124a target genes *in vitro*[4,5], and an increase of *Ptbp1* mRNA was observed in the telencephalon of a *Dicer* conditional knockout mouse[5]. *In vivo* knockdown of miR-124a in mouse SVZ cells identified *Sox9*, a neurogenesis suppressor gene, as a miR-124a target, suggesting that miR-124a controls neurogenesis through suppression of *Sox9* translation[6]. One study found that miR-124a is required for neuronal determination in the developing chick neural tube[4]. On the other hand, another study reported that miR-124a is not involved in the initial neuronal differentiation in the developing chick spinal cord[7]. A *Dicer* conditional knockout mice exhibited initial neurogenesis in the absence of miRNA production[8,9]. Considering these inconsistent observations, the target genes of miR-124a and its functional role in neural differentiation remain ambiguous.

RESULTS

Rncr3 is the dominant source of miR-124a

Previously, we used a screen to identify functionally important molecules in the retina[10] and isolated mouse *Rncr3* cDNA[11], which is highly expressed in the retina. We examined the expression profiles of *Rncr3* by northern blot analysis and detected a ~4.1-kb full-length *Rncr3* band specifically in the CNS tissues (**Fig. 1a**). We identified a stem loop of precursor miR-124a-1 (pre-miR-124a-1), which is encoded in exon of *Rncr3*. *Rncr3* fulfilled certain criteria for being a miR-124a precursor, including high expression in the brain, nuclear localization and the presence of a consensus sequence[12] (data not shown). We examined the expression patterns of *pre-miR-124a* and *miR-124a* and confirmed that they were specifically expressed in the CNS, including the retina (**Fig. 1b**). We then investigated the localization of *Rncr3* and miR-124a in the developing retina and brain using *in situ* hybridization (**Fig. 1c–i**). Both *Rncr3* and miR-124a signals were strongly detected in ganglion cells and differentiating neurons at embryonic day 13.5 (E13.5; **Fig. 1c,f**), and those signals gradually increased until the mice were 1 month old (**Fig. 1d,e,g,h**). The abundant miR-124a signals in photoreceptor cells accumulated in the inner segment from postnatal day 1 (P1) to adulthood (1 month of age; **Fig. 1g,h**). In the adult mice, the miR-124a signal was detected in differentiated neurons, except for putative Müller glial cells in the inner nuclear layer (**Fig. 1e,h**), consistent with previous findings[13]. In the P6 brain, *Rncr3* RNA was broadly expressed, especially in the hippocampus and the upper third of the cortex (**Fig. 1i**). These results suggest that *Rncr3* is specifically expressed in the CNS and functions as a primary miR-124a-1 (pri-miR-124a-1).

To determine the function of miR-124a *in vivo*, we generated *Rncr3*$^{-/-}$ mice by replacing all of the exons of *Rncr3* with the *PGK-neo* cassette (**Fig. 2a–c**). *Rncr3*$^{-/-}$ mice were initially viable and appeared to be normal; however, about two-thirds of the *Rncr3*$^{-/-}$ mice gradually

[1]Department of Developmental Biology, Osaka Bioscience Institute, Suita, Osaka, Japan. [2]Japan Science and Technology Agency (JST), Core Research for Evolutional Science and Technology (CREST), Osaka Bioscience Institute, Suita, Osaka, Japan. [3]Department of Molecular Neuroscience, Graduate School of Medicine, Osaka University, Suita, Osaka, Japan. [4]Department of Ophthalmology, Nagoya University Graduate School of Medicine, Showa-ku, Nagoya, Japan. [5]Department of Biological Sciences, Faculty of Medicine, Graduate School of Biostudies, Kyoto University, Yoshida, Sakyo-ku, Kyoto, Japan. [6]Department of Molecular Behavioral Biology, Osaka Bioscience Institute, Suita, Osaka, Japan. Correspondence should be addressed to T.F. (furukawa@obi.or.jp).

Received 2 May; accepted 30 June; published online 21 August 2011; doi:10.1038/nn.2897

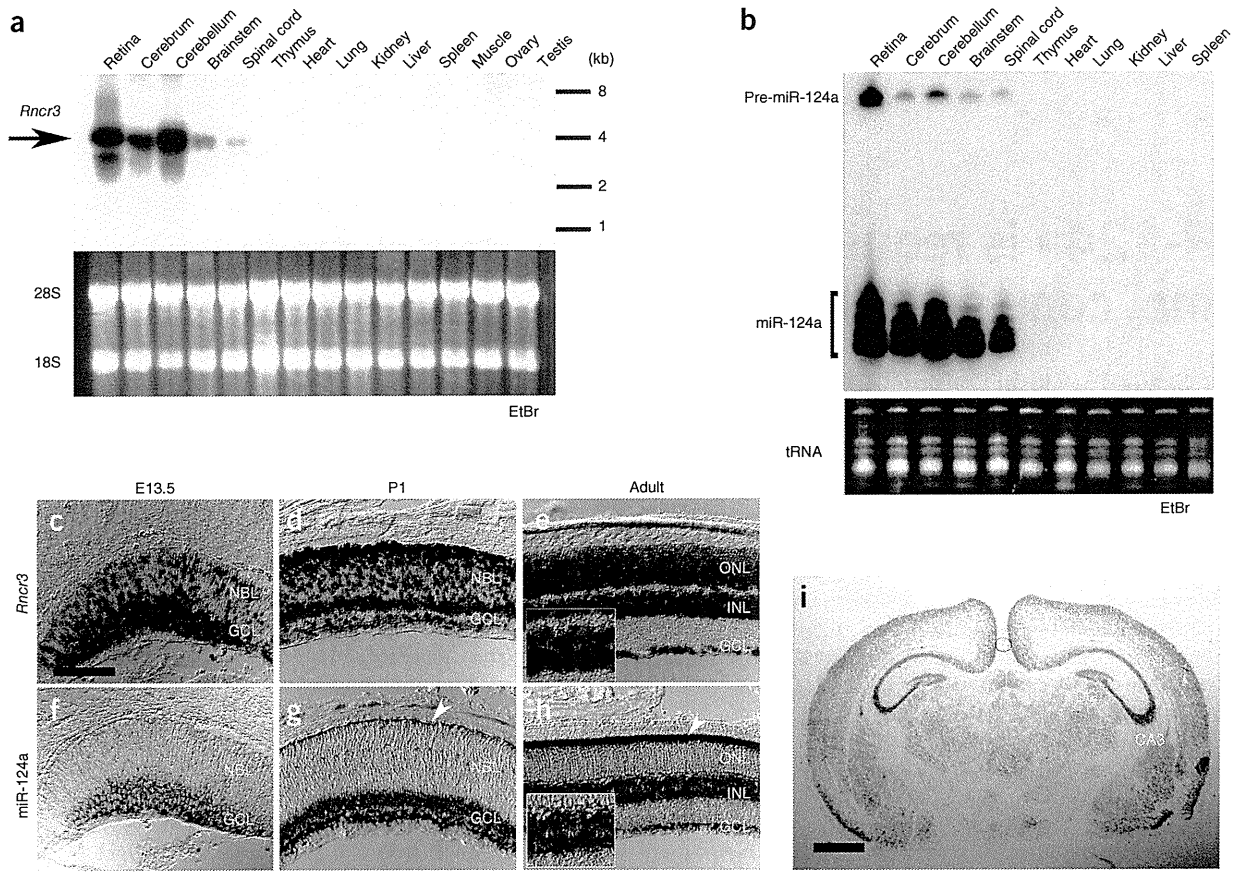

Figure 1 Expression of *Rncr3* and miR-124a. (**a**) Northern blot analysis of *Rncr3* transcripts in adult mouse tissues. The arrow indicates the approximately 4.1-kb *Rncr3* full-length mRNA. The lower panel shows ethidium bromide (EtBr) staining of RNA. (**b**) Northern blot analysis of miR-124a in adult mouse tissues. The upper panel shows miR-124a signals obtained from LNA-modified anti–miR-124a probe. The lower panel shows EtBr staining of small RNA. (**c–h**) Expression of *Rncr3* (**c–e**) and miR-124a (**f–h**) was detected by *in situ* hybridization in the developing retina at E13.5 (**c**,**f**), P1 (**d**,**g**) and in adult mice (1 month old, **e**,**h**). miR-124a signal was detected in the developing photoreceptor layer at P1 and the inner segments of photoreceptors in adults (**g** and **h**, arrowheads). The small boxes in **e** and **h** show unstained blank spots by *in situ* hybridization, which may correspond to Müller glia cells in the inner nuclear layer (INL). Scale bar represents 100 μm. (**i**) Expression of *Rncr3* in the developing brain at P6. Scale bar represents 1 mm. CTX, cortex; DG, dentate gyrus; GCL, ganglion cell layer; NBL, neuroblastic layer; ONL, outer nuclear layer.

became debilitated and died around P20 for unknown reasons. We compared miR-124a expression among wild-type, $Rncr3^{+/-}$ and $Rncr3^{-/-}$ mice and found that miR-124a band intensities were substantially reduced by 60–80% in all of the $Rncr3^{-/-}$ CNS regions that we examined at P14 (**Fig. 2d**). We then performed northern blots for miR-124a and an absolute quantitative RT-PCR (qPCR) assay for pri-miR-124a-1, pri-miR-124a-2 and pri-miR-124a-3 using the retina, hippocampus and cortex of P6 wild-type and $Rncr3^{-/-}$ mice (**Supplementary Fig. 1**). miR-124a expression was reduced by 60–80% in $Rncr3^{-/-}$ mice (**Supplementary Fig. 1a**) and pri-miR-124a-3 was undetectable in both wild-type and $Rncr3^{-/-}$ mice (**Supplementary Fig. 1b**), indicating that *Rncr3* (pri-miR-124a-1) is the dominant source of miR-124a.

We then examined the tissue distribution of miR-124a in developing $Rncr3^{-/-}$ mice using *in situ* hybridization to identify tissues in which miR-124a knockout was not compensated for by expression of pre-miR-124a-2 or pre-miR-124a-3. miR-124a expression was substantially reduced and barely detectable in the presumptive photoreceptor layer (PPL), where cone photoreceptor neurogenesis occurs from E11 to E18 (refs. 14,15), of $Rncr3^{-/-}$ retina at E15.5 (**Fig. 2e–h**), whereas NEUROD1, a neuronal differentiation and early photoreceptor marker, was detected at normal levels (wild type, 908.5 ± 58.2 cells per section; $Rncr3^{-/-}$, 919 ± 33.8; $P = 0.79$; **Fig. 2i–l**). In the E17.5 wild-type retina, pri-miR-124a-1 (*Rncr3*) was strongly observed in the PPL; however, the pri-miR-124a-2 host gene was barely expressed and pri-miR-124a-3 was undetectable (**Supplementary Fig. 2a–f**), suggesting that pri-miR124a-1 is the predominant source of miR-124a in the PPL.

We next observed sections of the P6 developing $Rncr3^{-/-}$ brain (**Fig. 2m–p**). The $Rncr3^{-/-}$ brain was smaller than that of the wild type, but its morphology was not substantially affected (**Fig. 2m**,**n**). miR-124a expression was significantly reduced in the $Rncr3^{-/-}$ brain compared with that in the wild-type brain, as determined by *in situ* hybridization (**Fig. 2o**,**p**). We found an especially substantial loss of miR-124a expression in the $Rncr3^{-/-}$ hippocampal dentate gyrus (**Fig. 2p**). Our results suggest that miR-124a expression is almost abolished in the developing cone photoreceptor layer and dentate gyrus in the hippocampus. Thus, we focused our analysis on retinal cone photoreceptors and the dentate gyrus.

Rncr3$^{-/-}$ mice exhibit neuronal dysfunction and dysmaturation

We first analyzed cone cells in the $Rncr3^{-/-}$ retina. We performed flat-mount immunostaining using 2-month-old $Rncr3^{-/-}$ retinas and

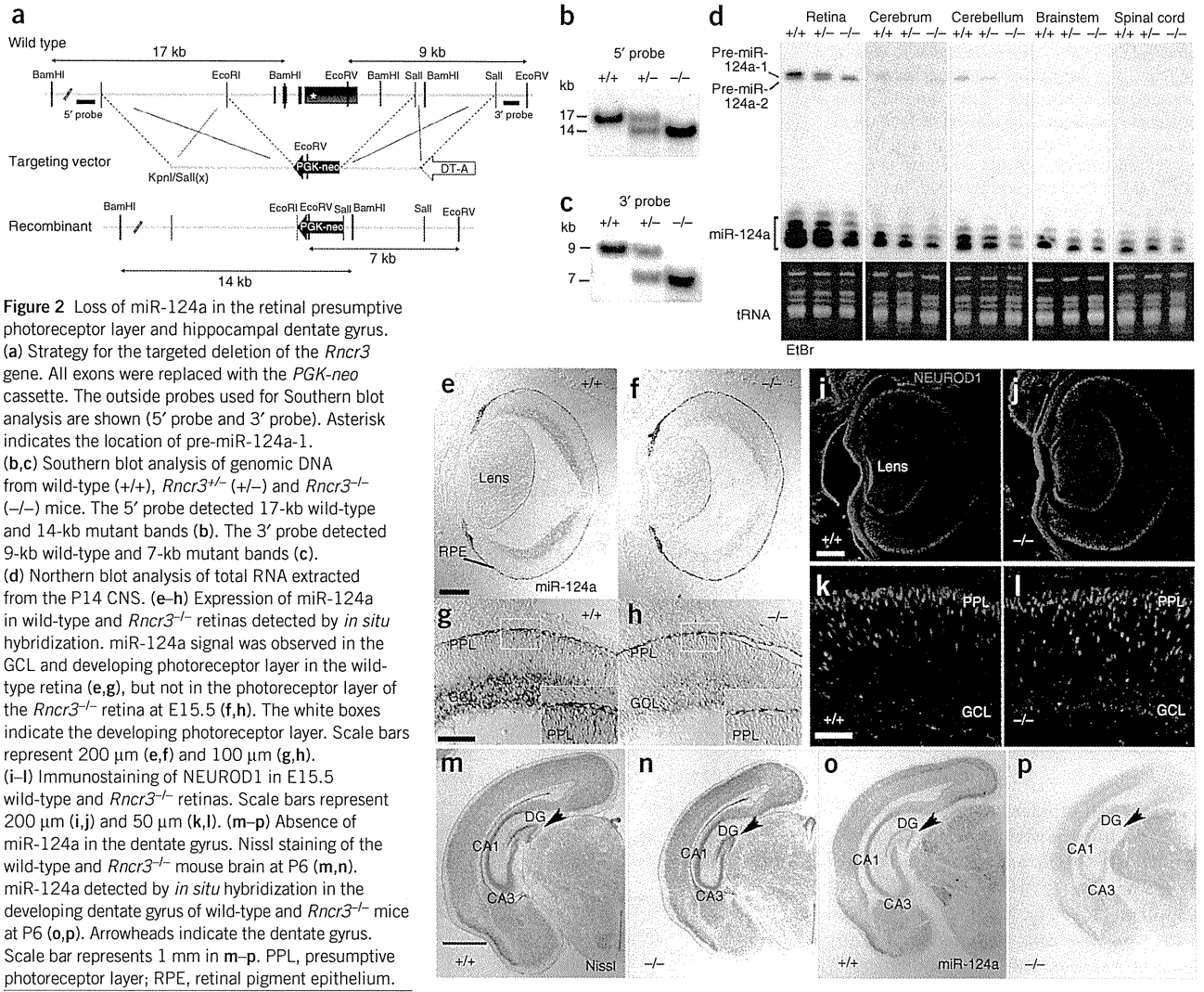

Figure 2 Loss of miR-124a in the retinal presumptive photoreceptor layer and hippocampal dentate gyrus. (**a**) Strategy for the targeted deletion of the *Rncr3* gene. All exons were replaced with the *PGK-neo* cassette. The outside probes used for Southern blot analysis are shown (5′ probe and 3′ probe). Asterisk indicates the location of pre-miR-124a-1. (**b**,**c**) Southern blot analysis of genomic DNA from wild-type (+/+), *Rncr3*$^{+/-}$ (+/−) and *Rncr3*$^{-/-}$ (−/−) mice. The 5′ probe detected 17-kb wild-type and 14-kb mutant bands (**b**). The 3′ probe detected 9-kb wild-type and 7-kb mutant bands (**c**). (**d**) Northern blot analysis of total RNA extracted from the P14 CNS. (**e**–**h**) Expression of miR-124a in wild-type and *Rncr3*$^{-/-}$ retinas detected by *in situ* hybridization. miR-124a signal was observed in the GCL and developing photoreceptor layer in the wild-type retina (**e**,**g**), but not in the photoreceptor layer of the *Rncr3*$^{-/-}$ retina at E15.5 (**f**,**h**). The white boxes indicate the developing photoreceptor layer. Scale bars represent 200 μm (**e**,**f**) and 100 μm (**g**,**h**). (**i**–**l**) Immunostaining of NEUROD1 in E15.5 wild-type and *Rncr3*$^{-/-}$ retinas. Scale bars represent 200 μm (**i**,**j**) and 50 μm (**k**,**l**). (**m**–**p**) Absence of miR-124a in the dentate gyrus. Nissl staining of the wild-type and *Rncr3*$^{-/-}$ mouse brain at P6 (**m**,**n**). miR-124a detected by *in situ* hybridization in the developing dentate gyrus of wild-type and *Rncr3*$^{-/-}$ mice at P6 (**o**,**p**). Arrowheads indicate the dentate gyrus. Scale bar represents 1 mm in **m**–**p**. PPL, presumptive photoreceptor layer; RPE, retinal pigment epithelium.

observed a significant reduction of the cone cell number and of mRNA expression of cone-specific genes ($P < 0.001$; **Fig. 3a–d**). To evaluate the physiological function of the *Rncr3*$^{-/-}$ retina *in vivo*, we recorded scotopic and photopic electroretinograms (ERGs) from 2-month-old wild-type and *Rncr3*$^{-/-}$ mice. Both the waveforms and amplitudes of a- and b-waves of scotopic ERGs were very similar between wild-type and *Rncr3*$^{-/-}$ mice (**Fig. 3e–g**). In contrast, the amplitudes of the photopic ERGs of *Rncr3*$^{-/-}$ mice were significantly smaller than those of wild-type mice at all stimulus intensities ($P < 0.05$; **Fig. 3h–j**). The amplitudes of the a-waves, which originate from cone photoreceptors, were less than one-third of those of wild-type mice. Moreover, we found that some opsin-positive cone cells were ectopically localized in the *Rncr3*$^{-/-}$ retina (**Supplementary Fig. 3a–g**). We also examined the development of other retinal cell types in 2-month-old *Rncr3*$^{-/-}$ mouse retinas by immunostaining (**Supplementary Fig. 4a–g**). Rod photoreceptor cells, bipolar cells, amacrine cells, horizontal cells, ganglion cells and Müller glial cells were unaffected. These results indicate that cone photoreceptors are impaired in *Rncr3*$^{-/-}$ mice.

In the developing mouse retina, the expression of TRβ2, an early cone marker, peaks at E17.5 (ref. 16). We examined the number of TRβ2-positive cells in the *Rncr3*$^{-/-}$ retina (**Supplementary Fig. 5a–c**). The number of cones was unaltered in the *Rncr3*$^{-/-}$ retina at E17.5 (**Supplementary Fig. 5c**). Notably, we found some mis-localized TRβ2-positive cells in the E17.5 mutant retina (**Supplementary Fig. 5b**). We then examined the expression of *Crx* and *Otx2*, photoreceptor cell differentiation genes[17–19], and *Neurogenin 2* (*Ngn2*, also known as *Neurog2*), a proneural gene, in both the wild-type and *Rncr3*$^{-/-}$ retinas at E13.5 by *in situ* hybridization and qPCR analysis (**Supplementary Fig. 5d–n**). In contrast with our cone number results, we found no apparent effect on early neurogenesis by quantitatively measuring *Neurod1*, *Trβ2*, *Crx*, *Otx2* and *Ngn2* in wild-type and *Rncr3*$^{-/-}$ retinas, although miR-124a expression was reduced (**Figs. 2i–m** and **3a–d** and **Supplementary Fig. 5a–n**). We examined apoptosis by TUNEL assay in wild-type and *Rncr3*$^{-/-}$ retinas, and found that the number of TUNEL-positive cells was significantly increased in the P3 *Rncr3*$^{-/-}$ retina ($P < 0.05$; **Supplementary Fig. 6a–c**). We further observed an increase in the number of TRβ2 and active caspase-3 double-positive cells and a decrease in the number of TRβ2-positive, caspase-3–negative cells in the *Rncr3*$^{-/-}$ retina (**Fig. 3k–p**), suggesting that the number of cone cells was reduced by apoptosis after neurogenesis. Furthermore, a recent study found that miR-124a was substantially reduced in anaplastic astrocytomas[20]. Thus, we

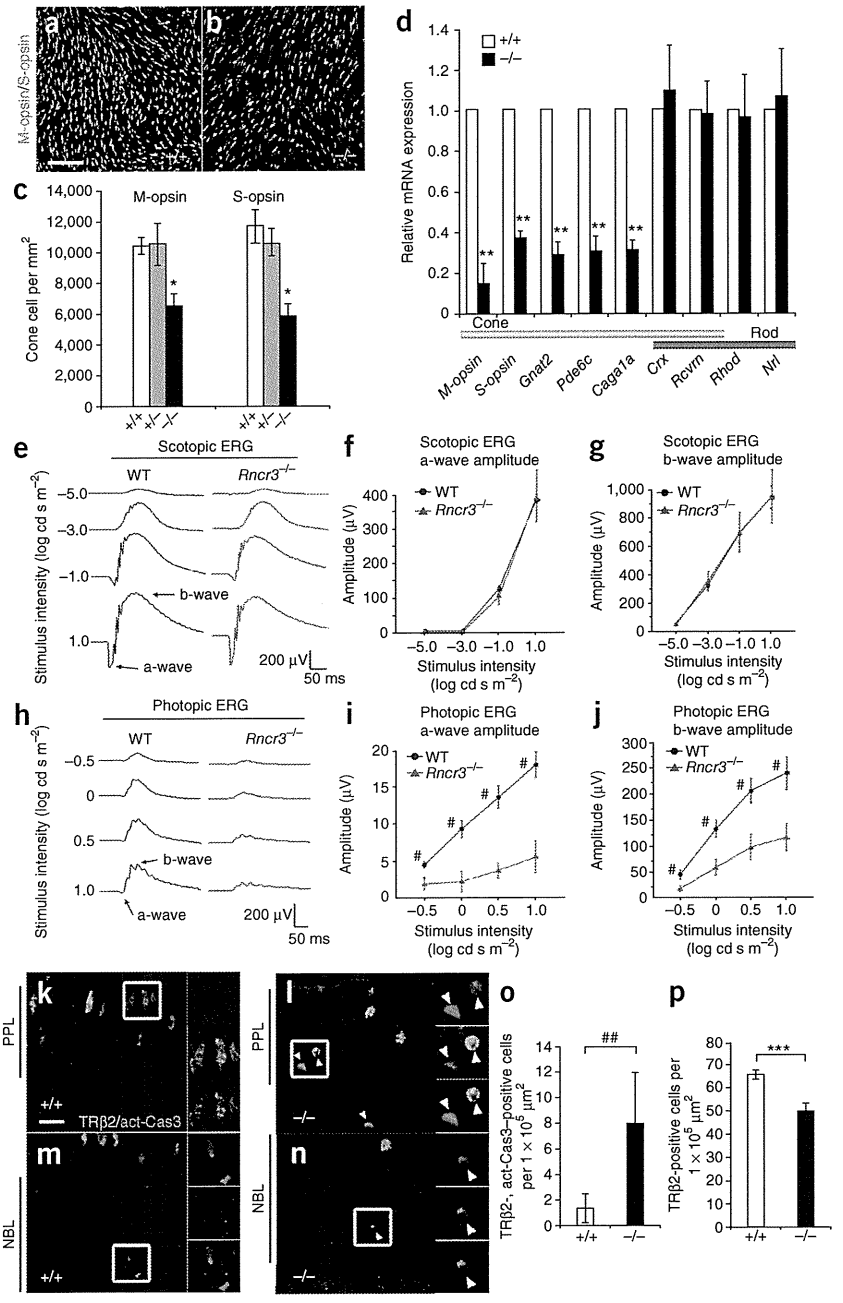

Figure 3 Reduction of cone photoreceptor cells in the *Rncr3*$^{-/-}$ retina. (**a–c**) Flat-mount immunostaining of central regions of wild-type (**a**) and *Rncr3*$^{-/-}$ (**b**) retinas using antibody to M-opsin (magenta) and antibody to S-opsin (green). Scale bar represents 50 μm. The number of cone cells expressing M-opsin and/or S-opsin in wild-type, *Rncr3*$^{+/-}$ and *Rncr3*$^{-/-}$ retinas are shown in **c** (*$P < 0.001$). Error bars represent s.d. from the means of triplicates. (**d**) Quantitative RT-PCR of retinal photoreceptor genes at P14 (**$P < 0.01$). Error bars represent s.d. from the means of three littermate pairs. *Actb* was used for normalization. (**e–j**) ERGs recorded from 2-month-old wild-type and *Rncr3*$^{-/-}$ mice. Scotopic ERGs elicited by four different stimulus intensities are shown in **e**. The amplitudes of the scotopic ERG a-wave (**f**) and the b-wave (**g**) are shown as a function of the stimulus intensity. Photopic ERGs elicited by four different stimulus intensities are shown in **h**. The amplitude of the photopic ERG a-wave (**i**) and the b-wave (**j**) are shown as a function of the stimulus intensity. Error bars represent s.e.m. (#$P < 0.05$). (**k–p**) Immunostaining of active caspase-3 (act-Cas3) and TRβ2 in the *Rncr3*$^{-/-}$ retina at P3. Arrowheads indicate active caspase-3 and TRβ2 double-positive cells. The white boxes indicate the area enlarged in the right panels. Scale bar represents 10 μm (**k–n**). The number of active caspase-3 and TRβ2 double-positive cells (**o**) and of TRβ2-positive cells (**p**) are shown. Error bars represent s.d. from the means of triplicates. ##$P < 0.02$, ***$P < 0.002$.

examined cell proliferation in the *Rncr3*$^{-/-}$ retina by immunostaining with phosphohistone H3 (PH3) and Ki67 and counting the number of PH3-positive cells at P3 (**Supplementary Fig. 7a–c**). The proportion of PH3-positive cells was not significantly different between wild-type and *Rncr3*$^{-/-}$ retinas ($P > 0.9$). These results suggest that miR-124a is necessary for proper survival and localization of cone cells rather than for early neurogenesis.

We found that 2-month-old *Rncr3*$^{-/-}$ mice had smaller brain weights than did wild types (**Fig. 4a,b**). The small brain phenotype was not apparent at P1, but became significant by P6 during maturation ($P < 0.005$, data not shown). Furthermore, *Rncr3*$^{-/-}$ mice exhibited a front and hind limb clasping response in the tail-suspension assay at 4–5 months (**Fig. 4c,d**). This abnormal phenotype is commonly observed in mouse models of neurodegenerative disorders[21], suggesting that the neural function of the *Rncr3*$^{-/-}$ mouse is substantially impaired. We then performed Timm staining on P10 wild-type and *Rncr3*$^{-/-}$ brain sections, the time at which mossy fibers develop[22], to examine dentate granule cell maturation (**Fig. 4e–h**). Notably, aberrant outgrowth of mossy fibers (dentate granule cell axons) into the CA3 region was observed in the *Rncr3*$^{-/-}$ mouse (**Fig. 4g,h**). The number of apoptotic cells in the dentate gyrus and cortex at P6 was significantly increased (dentate gyrus: wild type, 1.2 ± 1.6 cells per section; *Rncr3*$^{-/-}$, 10.2 ± 3.6; $P < 0.001$; cortex: wild type, 5.8 ± 2.5 cells per 5×10^5 μm^2; *Rncr3*$^{-/-}$, 59.4 ± 17.1; $P < 0.001$; **Fig. 4i–l**). Cell proliferation in the dentate gyrus of *Rncr3*$^{-/-}$ mice was not substantially affected (**Supplementary Fig. 7d,e**), suggesting that apoptosis of neurons contributes to the smaller brain size in *Rncr3*$^{-/-}$ mice. These results indicate that miR-124a is necessary for proper brain development and axogenesis of dentate granule neurons to the CA3.

Lhx2 is a direct target mRNA of miR-124a *in vivo*

To identify miR-124a target mRNAs, we searched for 3′ untranslated regions (UTRs) of genes that are highly expressed in retinal progenitors and substantially downregulated on progenitor differentiation[23], such as *Lhx2*, *Sox2*, *Rax*, *Six6*, *Six3*, *Pax2*, *Pax6*, *Vsx2* and *Otx2*, using TargetScan 5.1 (http://www.targetscan.org/). Searching the database revealed that *Lhx2* contains an evolutionarily

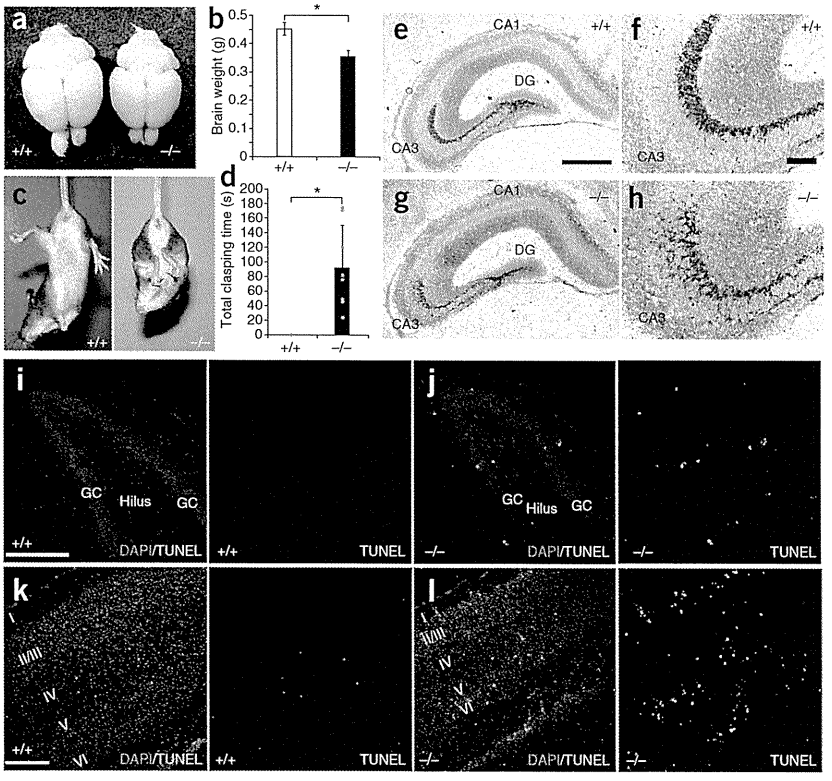

Figure 4 *Rncr3*$^{-/-}$ mice exhibit neuronal dysfunction and aberrant growth of dentate granule cell axon. (**a**,**b**) Appearance of the brain and brain weight in wild-type and *Rncr3*$^{-/-}$ mice. Representative brains from wild-type (left) and *Rncr3*$^{-/-}$ mice (right, litter mates, 2 months old) are shown in **a**. Brain weights of wild-type ($n = 5$) and *Rncr3*$^{-/-}$ mice ($n = 9$) are shown in **b** (*$P < 0.001$). Error bars represent s.d. (**c**,**d**) Abnormal limb-clasping of *Rncr3*$^{-/-}$ mouse. A clasping response was observed in the *Rncr3*$^{-/-}$ mouse (**c**, right), but not in the wild-type mouse (**c**, left). Total clasping time was measured for 3 min (**d**). Error bars represent s.d. from the mean of $n = 4$ (wild type) and $n = 8$ (*Rncr3*$^{-/-}$). (**e**–**h**) Aberrant sprouting of mossy fibers in the *Rncr3*$^{-/-}$ mouse. The mossy fiber terminals were visualized by Timm staining with Nissl counterstaining at P10. Scale bars represent 500 μm (**e**,**g**) and 100 μm (**f**,**h**). (**i**,**j**) TUNEL assay of the P6 wild-type and *Rncr3*$^{-/-}$ dentate gyrus. Scale bars represent 200 μm. (**k**,**l**) TUNEL assay of the P6 wild-type and *Rncr3*$^{-/-}$ visual cortex. Scale bars represent 200 μm. GC, granule cell layer.

highly conserved miR-124a target sequence (**Fig. 5a**). We examined whether *Lhx2* is a target mRNA of miR-124a by constructing luciferase reporter plasmids that contained native or mutated seed sequences of the *Lhx2* 3′ UTR (**Fig. 5a**) and co-transfecting these reporter plasmids with miR-124a expression plasmids (*pBAsi-mU6-miR-124a-1*, *pBAsi-mU6-miR-124a-2* or *pBAsi-mU6-miR-124a-3*) into HEK 293T cells that lacked endogenous miR-124a (**Supplementary Fig. 8a**,**b**). HEK 293T cells transfected with miR-124a expression plasmids produced significant amounts of miR-124a ($P < 0.001$; **Supplementary Fig. 8a**,**b**). The luciferase activity of the native *Lhx2* 3′-UTR plasmid was significantly reduced by all of the pre-miR-124a expression plasmids ($P < 0.01$; **Fig. 5b**). However, luciferase activity of the mutated *Lhx2* 3′-UTR plasmid was not attenuated by miR-124a (**Fig. 5b**), and the luciferase mRNA levels of both native and mutated *Lhx2* 3′-UTR plasmids were not significantly reduced ($P < 0.004$; **Supplementary Fig. 8c**,**d**). We observed a statistically significant increase of luciferase activity in *Rncr3*$^{-/-}$ hippocampal neurons transfected with native Lhx2 3′-UTR plasmid ($P < 0.009$), but found no significant effect in neurons transfected with the mutated *Lhx2* 3′-UTR plasmid ($P > 0.45$; **Supplementary Fig. 8e**). Next, to determine whether *Lhx2* is an *in vivo* target of miR-124a, we performed immunostaining of the E17.5 *Rncr3*$^{-/-}$ retina using antibodies to LHX2 and TRβ2 antibodies (**Fig. 5c–e**). The number of LHX2 and TRβ2 double-positive cells was significantly increased in the *Rncr3*$^{-/-}$ retina compared with the wild-type retina ($P < 0.01$; **Fig. 5e**). We then introduced *Lhx2* expression plasmids that contained native or mutated 3′ UTR (*Lhx2-Nat* and *Lhx2-Mut*) together with an *egfp* expression plasmid into the P0 mouse retina by *in vivo* electroporation to determine whether retinal cell apoptosis occurs by *Lhx2* overexpression. The number of TUNEL-positive cells was increased in retina transfected with the *Lhx2-Mut* plasmid, but transfection with the *Lhx2-Nat* plasmid did not lead to an increase in the number of TUNEL-positive cells (**Fig. 5f–h**), suggesting that the native 3′ UTR was targeted by native miR-124a. This result is consistent with the observation that the number of TUNEL-positive cells was significantly increased in the *Rncr3*$^{-/-}$ retina ($P < 0.05$; **Supplementary Fig. 6a–c**). These results suggest that *Lhx2* mRNA is a miR-124a target in the retina and that downregulation of *Lhx2* mRNA by miR-124a is necessary for retinal cell survival.

Lhx2 is known to be required for hippocampal formation[24]. We therefore conducted immunostaining on the dentate gyrus with antibodies to LHX2 and the dentate gyrus marker PROX1. The number of LHX2 and PROX1 double-positive cells was significantly increased in the *Rncr3*$^{-/-}$ dentate gyrus ($P < 0.001$; **Fig. 5i–k**). Furthermore, we compared the expression of *Rncr3* and *Lhx2* mRNA and LHX2 protein in the E12.5 forebrain and P3 retina (**Supplementary Fig. 8f–o**). At E12.5, *Lhx2* mRNA was highly expressed in both the hippocampus and thalamus, whereas *Rncr3* was highly expressed only in the thalamus. In both the developing brain and retina, LHX2 protein was not expressed in regions in which both *Lhx2* and *Rncr3* mRNA were expressed, suggesting that miR-124a targets *Lhx2* mRNA both in the retina and the brain and that miR-124a inhibits translation of *Lhx2* mRNA. Cell density was significantly higher in the dentate gyrus in *Rncr3*$^{-/-}$ mice than in wild-type mice, as determined by counting PROX1-positive cells ($P < 0.004$; **Fig. 5i**,**j**,**l**). To assess the role of *Lhx2* in aberrant mossy fiber sprouting, we electroporated *Lhx2-Nat* and *Lhx2-Mut* plasmids into primary cultured hippocampal cells. Substantial neurite extension was observed in cells expressing *Lhx2-Mut* (**Fig. 5m–o**). To evaluate axonal elongation in dentate granule cells, we immunostained hippocampal PROX1 neurons and then measured the axonal length of PROX1-positive cells (**Fig. 5p**,**q**). The percentage of neurons that contained longer axons, greater than 150 μm in length, was increased by expression of *Lhx2-Mut* (**Fig. 5p**). Furthermore, the average length of the neurons in the top 25th percentile of the population was also significantly increased in *Lhx2-Mut*–expression neurons ($P < 0.05$; **Fig. 5q**). We ectopically expressed *Lhx2* using lentivirus in P6 rat dentate gyrus in slice culture and found that *Lhx2*-transduced dentate granule cells extended longer

axons to the CA3 region by 5 d *in vitro* (DIV) than the wild-type cells (**Fig. 5r–u**). These results suggest that a proper LHX2 protein level, which is affected by miR-124a, is required for the appropriate development of axons in the dentate gyrus.

Rescue of *Rncr3*$^{-/-}$ mice by pre-miR-124a-2 or *Lhx2* knockdown

To determine whether miR-124a is responsible for the *Rncr3*$^{-/-}$ retinal phenotype, we carried out a rescue experiment by mating *Rncr3*$^{-/-}$ mice with transgenic mice that specifically expressed miR-124a in

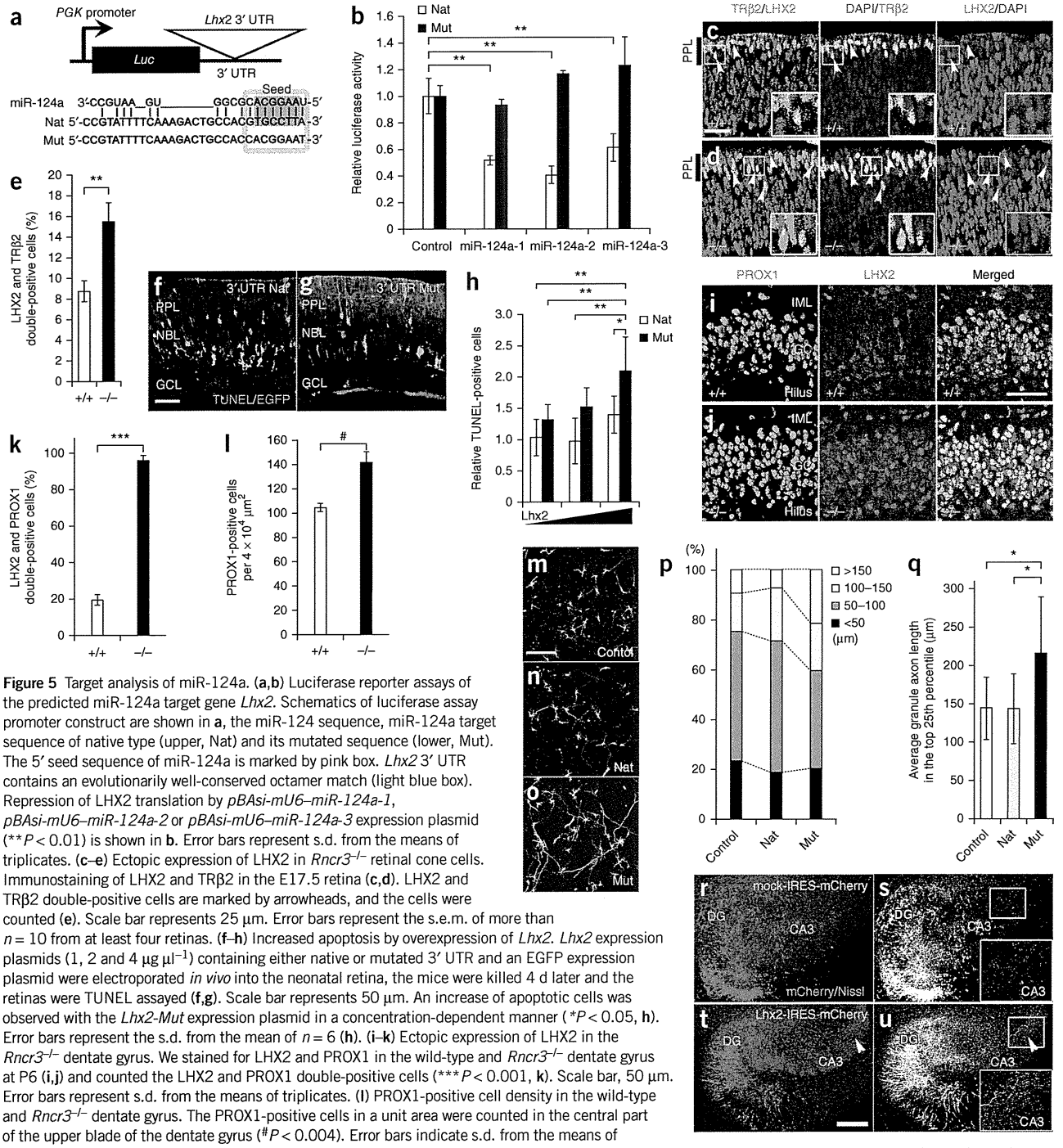

Figure 5 Target analysis of miR-124a. (**a**,**b**) Luciferase reporter assays of the predicted miR-124a target gene *Lhx2*. Schematics of luciferase assay promoter construct are shown in **a**, the miR-124 sequence, miR-124a target sequence of native type (upper, Nat) and its mutated sequence (lower, Mut). The 5′ seed sequence of miR-124a is marked by pink box. *Lhx2* 3′ UTR contains an evolutionarily well-conserved octamer match (light blue box). Repression of LHX2 translation by *pBAsi-mU6–miR-124a-1*, *pBAsi-mU6–miR-124a-2* or *pBAsi-mU6–miR-124a-3* expression plasmid (**$P < 0.01$) is shown in **b**. Error bars represent s.d. from the means of triplicates. (**c**–**e**) Ectopic expression of LHX2 in *Rncr3*$^{-/-}$ retinal cone cells. Immunostaining of LHX2 and TRβ2 in the E17.5 retina (**c**,**d**). LHX2 and TRβ2 double-positive cells are marked by arrowheads, and the cells were counted (**e**). Scale bar represents 25 μm. Error bars represent the s.e.m. of more than $n = 10$ from at least four retinas. (**f**–**h**) Increased apoptosis by overexpression of *Lhx2*. *Lhx2* expression plasmids (1, 2 and 4 μg μl^{-1}) containing either native or mutated 3′ UTR and an EGFP expression plasmid were electroporated *in vivo* into the neonatal retina, the mice were killed 4 d later and the retinas were TUNEL assayed (**f**,**g**). Scale bar represents 50 μm. An increase of apoptotic cells was observed with the *Lhx2-Mut* expression plasmid in a concentration-dependent manner (*$P < 0.05$, **h**). Error bars represent the s.d. from the mean of $n = 6$ (**h**). (**i**–**k**) Ectopic expression of LHX2 in the *Rncr3*$^{-/-}$ dentate gyrus. We stained for LHX2 and PROX1 in the wild-type and *Rncr3*$^{-/-}$ dentate gyrus at P6 (**i**,**j**) and counted the LHX2 and PROX1 double-positive cells (***$P < 0.001$, **k**). Scale bar, 50 μm. Error bars represent s.d. from the means of triplicates. (**l**) PROX1-positive cell density in the wild-type and *Rncr3*$^{-/-}$ dentate gyrus. The PROX1-positive cells in a unit area were counted in the central part of the upper blade of the dentate gyrus (#$P < 0.004$). Error bars indicate s.d. from the means of triplicates. (**m**–**q**) Axonal extension in *Lhx2-Mut*–expressing neurons. Primary hippocampal neurons from P0 mouse were transfected with mock (control), *Lhx2-Nat* (native), *Lhx2-Mut* (mutated) together with EGFP by electroporation. Confocal microimages of neurons 72 h after transfection are shown in **m**–**o**. Scale bar represents 200 μm. The percentages of axons with lengths ≤50, 50–100, 100–150 and >150 μm from $n = 85$ (control), 81 (nat), and 89 (mut) neurons are shown in **p**. The average axon lengths in the top 25% percentile are shown in **q**. Error bars represent s.d. (**r**–**u**) Lentivirus-infected hippocampal slice culture. Shown are confocal images of the P6, 5 DIV sliced rat hippocampus infected with mock (control, **r**,**s**) or *Lhx2* (**t**,**u**) expression virus. The small white boxes in **s** and **u** are the CA3 regions, magnified in the bottom right corner. Arrowheads indicate elongated mossy fibers in the CA3. Scale bar represents 200 μm. IML, inner molecular layer.

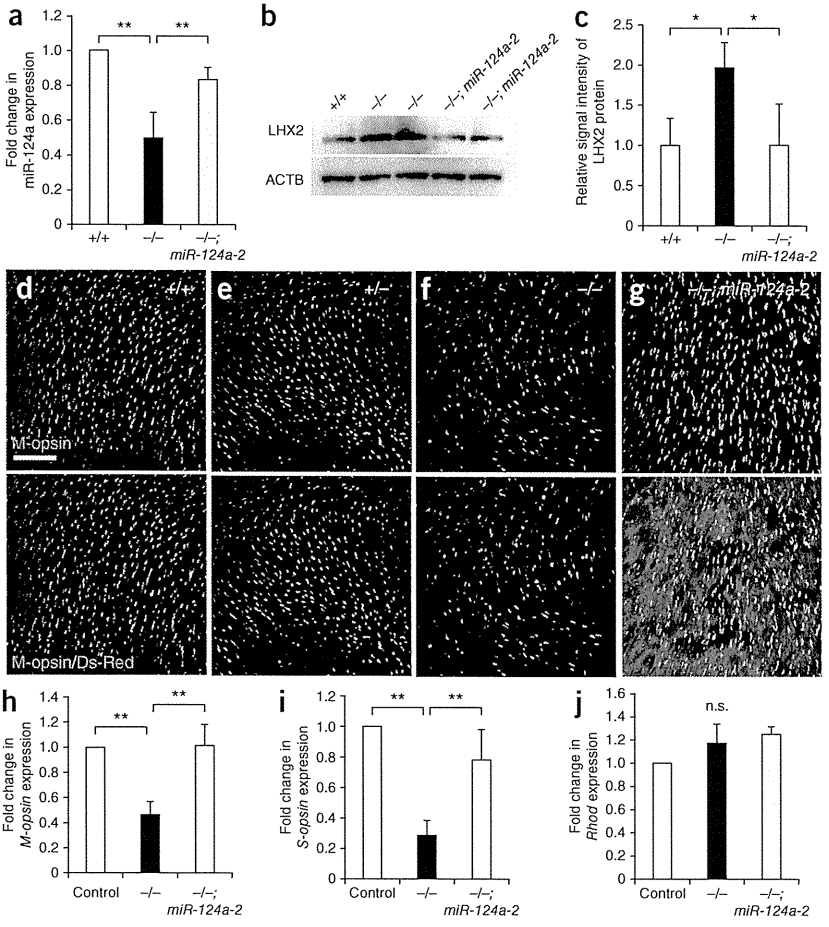

Figure 6 *In vivo* rescue experiments of *Rncr3*$^{-/-}$ mice by miR-124a expression in the retina. (**a**) Expression of miR-124a in the wild-type, *Rncr3*$^{-/-}$ and *Rncr3*$^{-/-}$; *Crx–miR-124a-2* retinas (**$P < 0.01$). Error bars represent the s.d. from the mean of triplicate (wild type and *Rncr3*$^{-/-}$) and $n = 4$ (*Rncr3*$^{-/-}$; *Crx–miR-124a-2*). (**b**,**c**) Comparison of LHX2 protein levels in the wild-type, *Rncr3*$^{-/-}$ and *Rncr3*$^{-/-}$; *Crx–miR-124a-2* retina. Western blots of LHX2 in the retina are shown in **b**. ACTB (β-actin) was used as a loading control. The signal intensity of LHX2 protein is shown in **c** (*$P < 0.05$). Error bars represent the s.d. from the means of triplicates (wild type) and $n = 4$ (*Rncr3*$^{-/-}$ and *Rncr3*$^{-/-}$; *Crx–miR-124a-2*). (**d–g**) Rescue of decreased cone cells by miR-124a expression. Flat-mount immunostaining using antibody to M-opsin (green). The *pre-miR-124a-2* transgene also expressed Ds-Red (magenta) as a marker. Scale bar represents 50 μm. (**h–j**) Real-time qRT-PCR analysis of control (+/+; *Crx–miR-124a-2* and *Rncr3*$^{+/-}$; *Crx–miR-124a-2*), *Rncr3*$^{-/-}$ and *Rncr3*$^{-/-}$; *Crx–miR-124a-2* transgenic retinas. Intron-spanning primers amplifying mouse *M-opsin* (also known as *Opn1mw*, **h**), *S-opsin* (also known as *Opn1sw*, **i**), *Rho* (**j**), and *Actb* were used for normalization. Error bars represent the s.d. from the means of three independent littermate pairs. **$P < 0.01$; n.s., not significant, $P > 0.05$.

photoreceptor cells using a *Ds-Red-intron-miR-124a-2* expression cassette driven by 2.3 kb of the *Crx* promoter[5,25] (*Crx–miR-124a-2*; **Supplementary Fig. 9a**). In the P1 retina, we observed that both miR-124a expression and the LHX2 protein level reverted back to those of control mice (**Fig. 6a–c**). We then performed flat-mount immunostaining (**Fig. 6d–g**) and conducted qPCR analysis on retinal photoreceptor marker genes using the adult retina (**Fig. 6h–j**). Both the decreased cone cell numbers and gene expression in the *Rncr3*$^{-/-}$ retina were restored to normal levels when transgenic pre-miR-124a-2 was expressed (**Fig. 6d–i**). The number of mislocalized cone cells also recovered (**Supplementary Fig. 9b–i**). These results suggest that the cone cell reduction and mislocalization in the *Rncr3*$^{-/-}$ retina are the results of miR-124a-1 disruption and that the primary function of *Rncr3* is to encode miR-124a.

To determine whether the loss of miR-124a is also responsible for the brain phenotypes, we generated a transgenic mouse that expresses *Ds-Red-intron-miR-124a-2* in postmitotic neurons, driven by 4.3 kb of the *synapsin 1* promoter (*Syn1–miR-124a-2*)[26] (**Supplementary Fig. 10a–c**). We performed an *in situ* hybridization of miR-124a and immunostained for LHX2 in the P10 brain. In the dentate gyrus of the *Rncr3*$^{-/-}$; *Syn1–miR-124a-2* mice, both the reduced level of mature miR-124a and the elevated level of LHX2 protein that we observed in *Rncr3*$^{-/-}$ mice were restored to similar levels as seen in control mice (**Fig. 7a–f**). In addition, the number of apoptotic cells was significantly reduced in the brains of *Rncr3*$^{-/-}$; *Syn1–miR-124a-2* mice compared with *Rncr3*$^{-/-}$ mice ($P < 0.01$; **Supplementary Fig. 10d**). In *Rncr3*$^{-/-}$; *Syn1–miR-124a-2* mice, Timm-stained mossy fiber axonal terminals incompletely, but substantially, recovered from aberrant sprouting into the CA3 region (**Fig. 7g–l**). The other phenotypes, including brain weight, clasping and apoptosis in the cortex, were not substantially rescued in *Rncr3*$^{-/-}$; *Syn1–miR-124a-2* mice (data not shown). This partial rescue may be a result of insufficient expression and/or inappropriate expression timing of the miR-124a transgene.

To determine whether downregulation of *Lhx2* can rescue the *Rncr3*$^{-/-}$ phenotype, we constructed a short hairpin RNA (shRNA) to knockdown *Lhx2* (*shLhx2*; **Supplementary Fig. 11a,b**). We transfected *shLhx2* into organ-cultured P0 retina using a recombinant adeno-associated virus serotype 5 (AAV5; **Supplementary Fig. 11c**). After 5 DIV, we performed immunostaining using an antibody to S-opsin. In the 5 DIV *Rncr3*$^{-/-}$ retina, the number of cone cells was reduced in retina transfected with control shRNA (shControl), whereas the number of cone cells was significantly increased in retina transfected with *shLhx2* compared with the control ($P < 0.01$; **Fig. 8a–e**). The number of cone cells in *shLhx2*-infected wild-type retina was unaltered (**Fig. 8a,c**), suggesting that the *Lhx2* knockdown rescue phenotype is not a result of an off-target effect. In addition, we forced the expression of shLhx2 in primary cultured hippocampal neurons to determine whether downregulation of *Lhx2* can rescue *Rncr3*$^{-/-}$ dentate gyrus neuron axonal elongation (**Fig. 8f–j**). The average dentate granular axon length in the neurons in the top 25th percentile of the population (determined by axon length) was significantly increased in shControl-transfected *Rncr3*$^{-/-}$ dentate gyrus neurons ($P < 0.01$; **Fig. 8g**). The elongated *Rncr3*$^{-/-}$ dentate gyrus axon phenotype was restored to the wild-type level by transfection of *shLhx2* (**Fig. 8i,j**). These results suggest that *Lhx2* is a primary target gene of miR-124a and is responsible for the *Rncr3*$^{-/-}$ phenotypes, including both the reduction of retinal cone cell numbers and mossy fiber elongation of the dentate gyrus.

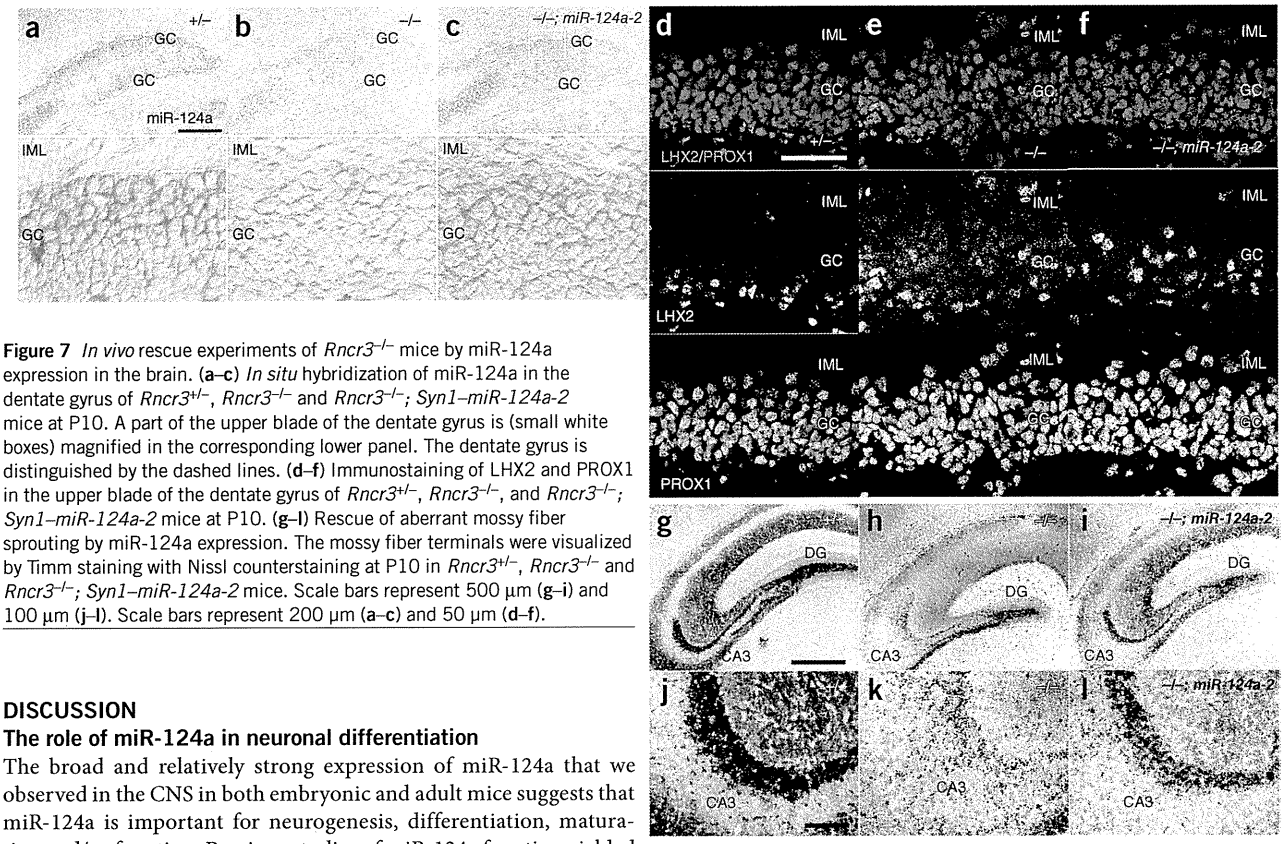

Figure 7 *In vivo* rescue experiments of *Rncr3*$^{-/-}$ mice by miR-124a expression in the brain. (**a–c**) *In situ* hybridization of miR-124a in the dentate gyrus of *Rncr3*$^{+/-}$, *Rncr3*$^{-/-}$ and *Rncr3*$^{-/-}$*; Syn1–miR-124a-2* mice at P10. A part of the upper blade of the dentate gyrus is (small white boxes) magnified in the corresponding lower panel. The dentate gyrus is distinguished by the dashed lines. (**d–f**) Immunostaining of LHX2 and PROX1 in the upper blade of the dentate gyrus of *Rncr3*$^{+/-}$, *Rncr3*$^{-/-}$, and *Rncr3*$^{-/-}$*; Syn1–miR-124a-2* mice at P10. (**g–l**) Rescue of aberrant mossy fiber sprouting by miR-124a expression. The mossy fiber terminals were visualized by Timm staining with Nissl counterstaining at P10 in *Rncr3*$^{+/-}$, *Rncr3*$^{-/-}$ and *Rncr3*$^{-/-}$*; Syn1–miR-124a-2* mice. Scale bars represent 500 μm (**g–i**) and 100 μm (**j–l**). Scale bars represent 200 μm (**a–c**) and 50 μm (**d–f**).

DISCUSSION

The role of miR-124a in neuronal differentiation

The broad and relatively strong expression of miR-124a that we observed in the CNS in both embryonic and adult mice suggests that miR-124a is important for neurogenesis, differentiation, maturation and/or function. Previous studies of miR-124a function yielded inconsistent results. A previous study found that miR-124a did not act as a determinant of neuronal generation through both knockdown and overexpression experiments of miR-124a in the developing chick neural tube[7]. In contrast, another study found that miR-124a is required for neuronal determination in the developing chick neural tube[4]. Studies using *Dicer* conditional knockout mice have shown that miRNA is not necessary for neuronal determination[8,9]. In *Xenopus*, a knockdown experiment by micro-injection of locked nucleic acid (LNA)–modified anti–miR-124a oligonucleotides into the eight-cell stage revealed no obvious effect[27]. We observed normal neurogenesis in the developing photoreceptor layer and the dentate gyrus in *Rncr3*$^{-/-}$ mice in which miR-124a expression is mostly eliminated. These results are consistent with previous reports that miR-124a is expressed in the Ki67-negative postmitotic cells and regulated by the REST complex[6,28], suggesting that miR-124a functions in neuronal maturation and maintenance, rather than neuronal determination (**Supplementary Fig. 12**). It will be important to examine the role of miR-124a in neuronal determination and maturation in the future,

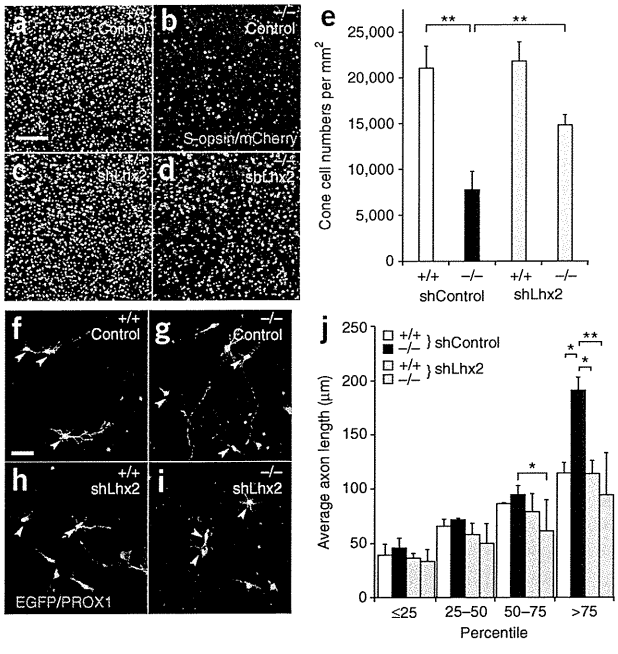

Figure 8 Rescue of *Rncr3*$^{-/-}$ mice by pre-miR-124a-2 expression. (**a–e**) Flat-mount immunostaining of S-opsin in the 5 DIV cultured retina. P0 wild-type (**a**,**c**) and *Rncr3*$^{-/-}$ retinas (**b**,**d**) were dissected and transfected with *U6* promoter–driven *shControl* (**a**,**b**) or *shLhx2* (**c**,**d**) with bicistronic expression of *CMV-mCherry* using AAV5 (**a–d**). Scale bar represents 50 μm. We counted the numbers of S-opsin–positive cone cell (**$P < 0.01$, **e**). Error bars represent s.d. from the means of $n = 4$. (**f–j**) Axon length of dentate granule cells after 70 h culture. P0 hippocampus of wild-type and *Rncr3*$^{-/-}$ mice were isolated and dissociated, then transfected with a *pBAsi-shControl* or *pBAsi-shLhx2-3* plasmid together with a *pCAG-egfp* plasmid. After immunostaining for PROX1 and EGFP, confocal fluorescence images were obtained. Scale bar represents 50 μm (**f–i**). The average axon length were calculated in 0–25th, 25–50th, 50–75th and 75–100th percentile groups (*$P < 0.05$ and **$P < 0.01$, **j**). Error bars represent s.d. from the means of $n = 3$. A total of 243 neurons were measured.